



A novel Nanocellulose-Gelatin-AS-IV external stent resists EndMT by activating autophagy to prevent restenosis of grafts

Tianshu Chu^{a,b,1}, Qingye Li^{c,1}, Chun Dai^{a,b,1}, Xiang Li^d, Xiang Kong^{a,b}, Yangming Fan^{a,b}, Hongyan Yin^a, Jianjun Ge^{a,b,*}

^a Department of Cardiac Surgery, The First Affiliated Hospital of USTC, Division of Life Sciences and Medicine, University of Science and Technology of China, Hefei, Anhui, 230001, China

^b Anhui Provincial Engineering Research Center for Cardiopulmonary and Vascular Materials, Hefei, Anhui, 230001, China

^c College of Food Science, Sichuan Agricultural University, No.46, Xin Kang Road, Yaan, Sichuan Province, 625014, PR China

^d CAS Key Laboratory of Soft Matter Chemistry, Department of Polymer Science and Engineering, University of Science and Technology of China, Hefei, Anhui, 230026, China

ARTICLE INFO

Keywords:

Restenosis
Vein graft
Extravascular stent
NC-Gelatin hydrogel
EndMT

ABSTRACT

Vein grafts are widely used for coronary artery bypass grafting and hemodialysis access, but restenosis remains the "Achilles' heel" of these treatments. An extravascular stent is one wrapped around the vein graft and provides mechanical strength; it can buffer high arterial pressure and secondary vascular dilation of the vein to prevent restenosis. In this study, we developed a novel Nanocellulose-gelatin hydrogel, loaded with the drug Astragaloside IV (AS-IV) as an extravascular scaffold to investigate its ability to reduce restenosis. We found that the excellent physical and chemical properties of the drug AS-IV loaded Nanocellulose-gelatin hydrogel external stent limit graft vein expansion and make the stent biocompatible. We also found it can prevent restenosis by resisting endothelial-to-mesenchymal transition (EndMT) *in vitro*. It does so by activating autophagy, and AS-IV can enhance this effect both *in vivo* and *in vitro*. This study has added to existing research on the mechanism of extravascular stents in preventing restenosis of grafted veins. Furthermore, we have developed a novel extravascular stent for the prevention and treatment of restenosis. This will help optimize the clinical treatment plan of external stents and improve the prognosis in patients with vein grafts.

1. Introduction

Vein grafts are commonly used for coronary artery bypass grafting and hemodialysis access. However, restenosis remains a major problem post these treatments [1,2]. After connection to the arterial system, the sudden increase in pressure in the grafted vein leads to intimal hyperplasia, which helps accumulate various inflammatory cells (such as macrophages, T cells, and B cells) at the site. These cells release various inflammatory factors, promoting the proliferation, transformation, and migration of vascular endothelial cells, smooth muscle cells, and fibroblasts to the grafted vein, eventually leading to the pathological process of neointima hyperplasia (NIH), resulting in a 1-year stenosis rate of up to 25% [3,4]. Autophagy is important for cells to maintain

self-homeostasis and to resist cellular and environmental pressure. Under physiological conditions, autophagy involves the degradation of harmful or surplus cellular components and provides them as nutrients or raw materials to lysosomes for cell recycling. However, under pathological conditions, autophagy acts as an adaptive response to stress to maintain homeostatic balance and constitutes a defense mechanism against adverse environments [5–8].

In our previous study, extravascular stents were able to inhibit endothelial-to-mesenchymal transition (EndMT) and thus inhibit restenosis of grafted veins [9]. EndMT is a complex process that contributes to neointimal formation in vein grafts. It is a process by which endothelial cells lose their characteristic phenotype and transform into a mesenchymal phenotype, including spindle-like morphological changes.

Peer review under responsibility of KeAi Communications Co., Ltd.

* Corresponding author. The First Affiliated Hospital of USTC, Division of Life Sciences and Medicine, University of Science and Technology of China, Hefei, 230001, China.

E-mail address: slgejianjun@outlook.com (J. Ge).

¹ These authors contributed equally to this work.

<https://doi.org/10.1016/j.bioactmat.2022.10.013>

Received 6 July 2022; Received in revised form 16 September 2022; Accepted 7 October 2022

2452-199X/© 2022 The Authors. Publishing services by Elsevier B.V. on behalf of KeAi Communications Co. Ltd. This is an open access article under the CC BY-NC-ND license (<http://creativecommons.org/licenses/by-nc-nd/4.0/>).

The mesenchymal form of the endothelial cells becomes more mobile, invasive, and contractile than typical endothelial cells. Moreover, they lose the ability to express the CD31-specific protein but can express smooth muscle actin (α -SMA) [10,11].

An extravascular stent is used around the grafted vein to provide resistance against high arterial pressure and to inhibit secondary vascular dilation. Furthermore, it reduces endothelial damage and inflammation by inhibiting macrophage accumulation, T cells, and other inflammatory cells and the release of inflammatory factors, thus inhibiting the process of EndMT and, therefore, prevents restenosis [12]. Recently, VEST clinical trials (Venous Extra Stent Technology) reported the good performance of an elastic alloy stent in inhibiting intimal hyperplasia of grafted veins; notably, this stent is non-degradable [13,14]. As a biodegradable and biocompatible polymer, gelatin has been widely used in tissue engineering [15–18]. Its chemical and physical stability has been achieved using the crosslinking agents formaldehyde, glutaraldehyde, and epoxy compounds; however, these agents exhibit a certain degree of physiological toxicity [19,20]. In contrast, genipin, a natural crosslinking agent from *Gardenia jasminoides*, shows low cytotoxicity and has been widely used for crosslinking various amino-containing polymer molecules [21–23]. Moreover, gelatin-based hydrogels, especially in the dry state, are brittle and unsuitable as extravascular stents. Nanocellulose (NC), a polysaccharide extracted mainly by acid hydrolysis of virgin cellulose, comprises repeating β -bound D-glucopyranosyl units and is commonly used to increase the toughness of hydrogels [24,25]. NC-Gelatin hydrogels have good mechanical properties and stability and are suitable as tissue engineering scaffolds and drug delivery systems [16,26,27]. Previously, we prepared NC-Gelatin hydrogels as extravascular stents and demonstrated that they are tough, provide sufficient mechanical support to the vein graft in the early stage after implantation, and are biocompatible [9,28,29]. Furthermore, extravascular stents resist EndMT through autophagy, thus preventing restenosis of grafted veins [9]. In vein grafting, the extravascular stent inhibits the secretion of IL-1 β , activates autophagy, reduces twist expression, inhibits the process of EndMT, inhibits NIH, and prevents restenosis of grafted veins [9,30]. Astragaloside-IV (AS-IV), one of the main components of Astragalus (*Astragalus membranaceus*), is commonly used in Chinese herbal medicine. Recently, clinical and experimental studies have shown that it can resist inflammation and activate autophagy [31–33].

In this study, we used a novel NC-Gelatin hydrogel as an extravascular stent to explore its potential mechanism for inhibiting restenosis. After performing *in vitro* experiments and *in vivo* implantation, we found that it has markedly good toughness and biocompatibility and inhibited intimal hyperplasia. Notably, it was able activate autophagy, resist EndMT, and inhibit restenosis. This effect was enhanced when loaded with AS-IV. Our results provide a new perspective for extravascular stents to prevent restenosis in grafted veins and reveal new targets, providing evidence for the clinical application of extravascular stents.

2. Materials and methods

2.1. Stent fabrication

Five grams of gelatin (9000-70-8; Aladdin, Shanghai, China) were added to 95 mL of distilled water and heated in a water bath at 60 °C. The mixture was stirred continuously until the gelatin was dissolved to obtain a 5% gelatin solution. Then, 0.5 g of genipin powder (6902-77-8; Aladdin) were added to 90.5 mL of distilled water and stirred at 25 °C until dissolved to obtain a 0.5% genipin solution and stored at 4 °C for later use. A certain amount of gelatin solution was measured and the genipin solution was added (relative to 3% of gelatin solid content); the mixture was ultrasonicated for 5 min until the two solutions were evenly mixed and kept for later use. NC was prepared according to the method reported by Akira Isogai et al. [34]. Briefly, 2 g of cork board were added to 400 mL of deionized water and dispersed by magnetic stirring. Then

0.032 g of TEMPO (2564-83-2; Aladdin) and 0.2 g of sodium bromide (98% purity; Aladdin) were added to the mixture and uniformly mixed by magnetic stirring. A certain amount of NaClO solution (10 mmol/g MFC) was added dropwise to the mixture at 25 °C to initiate TEMPO oxidation. In the TEMPO oxidation reaction, NaOH solution was added dropwise to maintain the pH value of the reaction mixture at approximately 10. The reaction was complete when the pH of the reaction mixture remained stable. Subsequently, the cellulose was washed repeatedly with deionized water until the water became neutral and a mixed aqueous solution of cellulose was prepared with a mass fraction of 0.3% (w/v). The NC suspension aqueous solution was stored at 4 °C until use. Subsequently, different concentrations of NC (0%, 5%, and 10% relative to the solid content of gelatin) were added to the gelatin-genipin solution, and the mixture was sonicated for 5 min to mix well, sealed in a disposable polystyrene Petri dish, and kept for 48 h at 25 °C and 50% humidity. Finally, the NC-Gelatin hydrogel extravascular stent was prepared by adding it to the mold. Subsequently, we have prepared 3 diameter molds, 4, 6, and 8 mm in diameter, each with a thickness of 0.3 mm and a length of up to 8 cm, tailored according to the conditions of use.

2.2. Fourier-transform infrared (FTIR) test

The stents were freeze-dried for FTIR analyses. We obtained the spectra with the OPUS software, and the spectra were recorded with a Nicolet 8700 FTIR instrument (Thermo Fisher, Waltham, MA, USA). The focus on the peak movement was set at 3300 cm⁻¹.

2.3. Scanning electron microscopy (SEM)

The stents were freeze-dried for SEM analyses. The micromorphology of the stents was imaged using a SEM (Gemini SEM500, Zeiss, Oberkochen, Germany).

2.4. Expansion analysis

The vein was placed on a PBS (phosphate buffered saline, PBS) operating table at a constant temperature of 37 °C, with the two ends connected, respectively, to a high-pressure syringe and a pressure gauge. The pressure ranged from 0 to 300 mmHg, and the Vernier calipers were used at five positions for the diameter recorded. This expansion test is based on the pressure control principle described by Professor Joyce Cheung-Flynn and the monitoring device described by Professor Hans Gregersen [35,36]. All procedures were performed under the Declaration of Helsinki of ethical standards of the 1964 and the First Affiliated Hospital of USTC (committee approved, Ethics No. 2021KY Ethical No. 51).

2.5. Thermogravimetric analysis (TGA)

The thermal stability of the stent was measured by TGA (Q600 SDT; TA Instruments; New Castle, DE, USA). All samples were heated from 20 to 220 °C at 10 °C/min. NETZSCH Proteus software (Version 4.8.5) was used for data analysis.

2.6. Cell co-culture and evaluation of the stent cell biocompatibility

Trypsin (C0201; Beyotime, Shanghai, China) was used for the digestion of human umbilical vein endothelial cells (HUVECs; Procell, China). After digestion, cell collection was completed via centrifugation and cells were suspended in the solution. Then, 100 μ L of cell suspension were taken and added to each well of a 96-well plate. Cells were grown in an incubator (37 °C with 5% CO₂) until confluence was reached. The stents were added to the wells and incubated for 24 h, 48 h, and 72 h for cell counting and Live/Dead test; and for 6 h, 12 h, 18 h, and 24 h for comet assay. PBS was added to the cells, washed once, and the cell

concentration was adjusted to 10^6 – 10^7 cells/mL after centrifugation. Agarose NMA, preheated at 56 °C, was dropped onto the preheated glass slide and placed at 4 °C for 15 min to solidify. Ten μ L of PBS containing 1000 cells and agarose LMA were mixed at 37 °C. The LMA containing cells were dropped onto the first layer of the gel plate and placed at 4 °C for 15 min to solidify. The slides were lysed upon immersion in cell lysis buffer for 1 h. After cell-lysis, cells were rinsed twice with PBS. Subsequently, the slides were placed in a horizontal electrophoresis tank and poured into the freshly prepared buffer. Alkali unwinding for 20 min was carried out in order to form single-stranded DNA. DNA strand scission was made to make it easier to migrate in the electrophoresis field. Electrophoresis was carried out at 25 v and 300 mA for 20 min. After electrophoresis, neutralization with Tris-HCl (pH 7.5) for 15 min was carried out. Then, 50 μ L of red fluorescent nucleic acid dye were added dropwise to each slide, protected from light, covered with a coverslip, and stained in the dark for 20 min before observation.

After culturing for different times, 10 μ L of CCK8 (BB-4202-01; Beibokit, Jiangsu, China) were added to each well and cultured for an additional 1 h. Single-cell suspensions with HUVECs were prepared, and then the electrophoresis and staining with fluorescent dyes were performed. Observing the degree of DNA damage under a fluorescent microscope and a Live/Dead Cell kit (BB-4126; Beibokit, Jiangsu, China) was conducted for the assessment of cell viability.

2.7. Evaluation of *in vivo* biocompatibility of the stent

All animal procedures obtained approval from the Ethics Committee of USTC (Ethics number: 2019-N(A)-086) and met the requirements of the National Institutes of Health Guide for the Care and Use of Laboratory Animals (NIH Publications No. 8023, revised 1978). All animals were purchased from the Animal Center of USTC. Mice (bodyweight: 25–35 g) were placed in rooms controlled by temperature and humidity in a 12/12-h light/dark cycle with food and water freely available. Following anesthesia for each mouse, the back skin was carefully incised and then the embeddedness of an external stent and the suture of the incision were performed. Mice were separated into two groups; post-surgery, one group was euthanized on day three and the other group was euthanized on day seven. Local tissue, heart, liver, spleen, kidney, and blood samples were collected from mice from both groups for follow-up experiments (immunohistochemistry analysis of local tissue for both groups for CD206, CD68, and iNOS; hematoxylin and eosin (H&E) staining and Masson staining of the heart, liver, spleen, lung, and kidney for both groups; flow cytometry analysis of the blood and spleen samples for both groups; Enzyme-linked immunosorbent assay (ELISA) IL-1 β (SU-B20174, RUIXIN BIOTECH, China), IL-2 (SU-B20176, RUIXIN BIOTECH, China), IL-6 (SU-B20188, RUIXIN BIOTECH, China), IL-4 (SU-B20186, RUIXIN BIOTECH, China), IL-10 (SU-B20162, RUIXIN BIOTECH, China), IL-13 (SU-B20167, RUIXIN BIOTECH, China) of blood samples for both groups; RT-PCR of spleen samples for both groups); H&E, Masson and immunohistochemistry (see section 2.10), and RT-PCR (see section 2.11). Spleen tissues were cut to form single-cell suspensions with added antibodies. Antibodies and red blood cell lysates (R1010; Solarbio) were added to the blood samples. The following antibodies were used: CD11B-PerCP-Cy5.5 (AH011B07-50, Liankebio, China), CD45R-PE-Cy7 (AM04510-50, Liankebio), CD3-FITC/CD45R-PE (AMC0501-50, Liankebio), and F4/80-APC (AM048005-50, Liankebio). The samples were tested on a CytoFLEX flow cytometer (Beckman Coulter). Mouse blood was centrifuged, and using ELISA kits to collect serum, IL-1 β (SU-B20174, Ruixinbio, China), IL-2 (SU-B20176, Ruixinbio), IL-4 (SU-B20186, Ruixinbio), IL-6 (SU-B20188, Ruixinbio), IL-10 (SU-B20162, Ruixinbio), and IL-13 (SU-B20167, Ruixinbio) were detected.

2.8. Surgical procedure and EndMT analysis

The rat autologous neck dynamic and static bypass model was used,

known as the “Cuff method” [9,29]. Briefly, Sprague-Dawley rats (males; aged 10 weeks, body weight: 200 g) were classified into six groups: vein, artery, graft, plus stent, stent loading low dose AS-IV, and stent loading high dose AS-IV. Four weeks after surgery, the grafted veins were removed for testing and these animals were euthanized.

EndMT was initiated by culturing the HUVECs in a medium, which contained 20% (v/v) Fetal Calf Serum, 1% (v/v) penicillin-streptomycin, 2 mM L-glutamine, 5 U/mL heparin, and 5(low)-15(high) ng/mL IL-1 β . After induction, the cells were collected four days later for testing.

2.9. Astragaloside-IV stent fabrication and release rate

We added 100 mg/mL (high dose) and 50 mg/mL (low dose) of AS-IV (84,687-43-4; Aladdin) to the prepared NC-Gelatin hydrogels, ultrasonically mixed them for 5 min to form a homogeneous suspension, and sealed them in a disposable polystyrene Petri dish at a temperature of 25 °C and a humidity of 50%. The solution was incubated for 48 h and then added to the stent mold to form an AS-IV stent. The AS-IV stent was placed in phosphate buffered saline (pH 7.5; 4 mL) and incubated at 37 °C. One milliliter of PBS was collected at indicated times, replaced by 1 mL of fresh PBS, and evaluated by liquid chromatography mass spectrometry (LC-MS-MS-8050; Shimadzu, Japan). We drew blood for concentration measurements 1, 3, 5, 10, 20, and 30 days after stent implantation. In terms of blood samples, serum was collected and centrifuged at 5000 rpm, and 1.8 mL of acetonitrile were added (LC-MS, Thermo Scientific™, MA, USA) per 200 μ L of serum to remove any trace of proteins. The filtered liquid was added to the injection vials and evaluated using a liquid chromatography mass spectrometer (LC-MS-MS-8050; Shimadzu).

2.10. Color Doppler ultrasonography

Four weeks after surgery, Color Doppler detection was performed in the rats to detect the blood flow to assess the patency rate of the grafted vein. After administering complete anesthesia, a Color Doppler Ultrasound of the blood vessels was performed (Resona R9; Mindray, Shenzhen, China) by placing the probe on the neck of the rats for blood flow detection.

2.11. Histomorphology, immunohistochemistry, and immunofluorescence

Three and seven days after surgery, local tissues at the site of the embedded stent were taken for H&E, Masson, and immunohistochemistry tests; the heart liver, spleen, lung, and kidney were taken for H&E and Masson staining. Four weeks after surgery, the grafted vein specimens were taken for H&E, Masson, and immunofluorescence tests. These samples were stored in formalin (G2161, Solarbio). After being soaked in hematoxylin dye solution (BA4041; Baso, Wuhan, China), samples were put in an eosin staining solution (BA-4022; Baso). After using the prepared hematoxylin samples, iron staining solution was used, the Masson blue solution (G1346; Solarbio) became blue again, and the magenta staining solution was added for 10 min. Samples were placed in aniline blue staining solution for 1–2 min, and a 95% ethanol and neutral glue seal were used for their rapid dehydration. ImageJ software was used for the quantitative analysis to assess the wall thickness, intimal thickness, intimal/wall, intimal area, lumen area, and intimal/lumen of the vein graft. The vein grafts were blocked with staining buffer for 1 h at 25 °C. To identify macrophages in local tissues, sections were incubated with the following antibodies: anti-CD68 (DF7518, Affinity, USA), anti-CD206 (DF4149, Affinity), and anti-iNOS (AF0199, Affinity). To identify the components of the vessel wall, the slices described above were incubated with the following antibodies: anti-CD31 (AF6191, Affinity), anti- α -smooth muscle actin (α -SMA; AF1032, Affinity), anti-LC3II (AF4650, Affinity), and anti-twist (AF4009, Affinity).

2.12. Reverse transcription quantitative polymerase chain reaction (RT-qPCR)

A slice of spleen tissue was ground into powder, lysed with 1 mL of TRIzol reagent (15596026; Thermo Fisher, USA), and centrifuged, producing a pellet and supernatant. RNA was extracted from the supernatant and turned into cDNA through reverse transcription using an ABI Step One Plus RT-qPCR system (Thermo Fisher). The gene expression was then determined for IL-1 β , IL-2, IL-6, IL-4, IL-10, and IL-13. Furthermore, a section of the vein graft was ground into powder, processed as described above, and gene expression was determined for IL-1 β , TGF- β , CD31, α -SMA, slug, snail 1, twist, vimentin, beclin1, LC3II, p62, AMPK, and mTOR. The EndMT system also detected these indicators. Results were determined using the $2^{-\Delta\Delta CT}$ method. The sequences of the primers are presented in [Supplementary Table 1](#).

2.13. Western blotting

Preprocessed samples were added to the RIPA lysate solution (P0013B; Beyotime, China), and the supernatants were collected after centrifugation. Samples were loaded onto sodium dodecyl sulfate-polyacrylamide gels (3250GR500; neoFROXX, Einhausen, Germany). Proteins were transferred to polyvinylidene difluoride membranes (WGPVDF22; Servicebio, China) after electrophoresis in transfer buffer for 5 min. The membranes were then incubated with primary antibodies (1:5000 dilution) targeting CD31 (AF6191, Affinity, USA), Vimentin (BF8006, Affinity), α -SMA (AF1032, Affinity), slug (350,136, ZENBIO, China), snail (AF6032, Affinity), twist (AF4009, Affinity), LC3II (3868S, CST, USA), p62 (AF5384, Affinity), beclin 1 (AF5128, Affinity), AMPK (AF6423, Affinity), p-AMPK (AF3423, Affinity), mTOR (AF6308, Affinity), and p-mTOR (AF3308, Affinity). Horseradish peroxidase-conjugated secondary antibodies at a 1:10,000 dilution were added

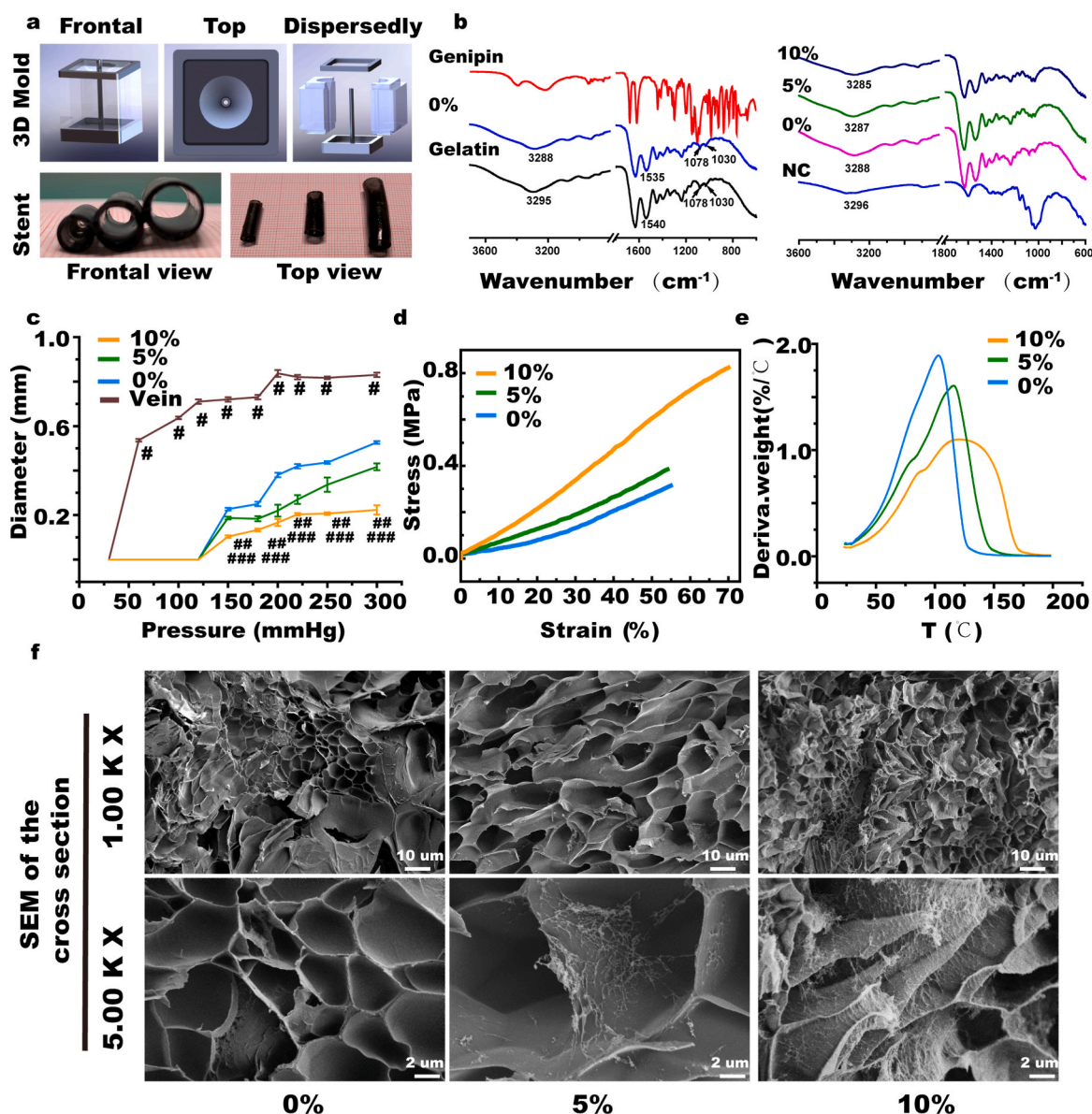


Fig. 1. Physical and chemical properties of the nanocellulose (NC)-Gelatin hydrogel extravascular stent. (a) The mold for the preparation of extravascular stents and the preparation of three diameter outer stents. (b) Fourier-transform infrared (FTIR) detection of nanocellulose, gelatin, genipin, and NC-hydrogels with different NC concentrations. (c) Expansion experiment of NC-hydrogels with different NC concentrations versus human saphenous vein. (d) The mechanical strength of the gelatin hydrogel further quantified with tensile testing. (e) TGA detection of NC-hydrogels with different NC concentrations. (f) Scanning electron microscopy (SEM) of NC-hydrogels with different NC concentrations. NS indicates not significant. # $p < 0.05$ (10% NC versus vein), ## $p < 0.05$ (10% NC versus 0% NC), ### $p < 0.05$ (10% NC versus 5% NC).

after washing. The membranes were then viewed with an automatic darkroom exposure instrument (JS-M6P; P&Q, China) and varying luminous intensities were used for optimal exposure.

2.14. Statistical analysis

Data are presented as means \pm standard deviations, which were processed by SPSS Version 21.0 (IBM, Chicago, IL, USA). For normally distributed data, one-way analysis of variance (ANOVA) was used to compare multiple groups. Fisher's least significant difference test was used to compare the two groups. Results with a p-value less than 0.05 were considered statistically significant.

3. Results

3.1. Fabrication and characterization of NC-Gelatin hydrogels extravascular stent

As shown in Fig. 1a and Supplementary Fig. S1, to adapt to the properties of the NC-Gelatin hydrogel, special extravascular stent mold was prepared, so that an extravascular stent of uniform thickness could be prepared. When fabricating the extravascular stent, we categorized the fabricated stents into different groups, namely 0% NC and 5% NC combined with 10% NC groups according to the different content of nanocellulose and determined the appropriate NC-Gelatin ratio through analysis of the physical and chemical properties. We then conducted subsequent experiments. As shown in Fig. 1b, FTIR observed a shift of the peak at 3300 cm^{-1} in the NC-Gelatin-gelatin hydrogel model, representing a combination of hydrogen bonds in the model. In the expansion experiment, the 10% NC group significantly inhibited the expansion of the grafted vein (10% NC: 0.103 ± 0.006 versus 5% NC: 0.186 ± 0.006 , 0% NC: 0.227 ± 0.006 , vein: 0.720 ± 0.010 mm, $p < 0.05$ at 150 mmHg; 10% NC: 0.167 ± 0.015 versus 5% NC: 0.220 ± 0.027 , 0% NC: 0.380 ± 0.010 , vein: 0.837 ± 0.015 mm, $p < 0.05$ at 200 mmHg; 10% NC: 0.207 ± 0.006 versus 5% NC: 0.337 ± 0.032 , 0% NC: 0.437 ± 0.006 , vein: 0.817 ± 0.006 mm, $p < 0.05$ at 250 mmHg) (Fig. 1c). The mechanical strength of the gelatin hydrogel was further quantified using tensile testing (Fig. 1d and Supplementary Figs. S1c, d, e, & f). The pure gelatin hydrogel exhibited poor mechanical performance with 0.315 MPa ultimate stress, 0.575 MPa tensile modulus, and 55% strain at break. The ultimate stress monotonically increased with increasing CNF content to 0.38, 0.71, and 0.82 MPa at 5%, 10%, and 15% CNF contents, respectively (Supplementary Fig. S1d). The 0.82 MPa ultimate stress of NFC-15% hydrogel was 2.6 times that of pure gelatin hydrogel. The 0.71 MPa ultimate stress of NFC-10% hydrogel was 1.9 times that of pure gelatin hydrogel. In addition, the Young's modulus also increased monotonically with increasing CNF content, reaching 1.17 MPa at 15% CNF content, 2.0 times that of pure gelatin hydrogel as well as 1.05 MPa at 10% CNF content, 1.8 times that of pure gelatin hydrogel. Surprisingly, the strain also increased to 70% at 15% CNF content (Supplementary Fig. S1f), which is 1.36 times that of the pure gelatin hydrogel. The strain also increased to 67% at 10% CNF content, which is 1.2 times that of the pure gelatin hydrogel. This indicates that the NC-hydrogel is not only stronger, but also tougher with 10% and 15% CNF content. In this experiment, the purpose of adding nanocellulose is to improve the mechanical properties and expansion strength of the hydrogel. As shown in Fig. 1c and Supplementary Figs. S1b, c, d, e, & f, when the content of nanocellulose was higher than 10%, the enhancement effect of cellulose on the mechanical properties and expansion of the composite hydrogel was not significant. In addition, an excessively high content of nanocellulose will increase the viscosity of the hydrogel, which is not conducive to its complete punching in a specific mold, and is prone to producing defected products. Therefore, considering the cost and comprehensive performance, 10% was selected as the experimental group in this study. There was little difference in the results of thermogravimetric analysis between the three

groups (Fig. 1e and Supplementary Fig. S2). Typical hydrogel-like morphology can be seen in the SEM of the three groups, and more nanocellulose can be seen enriched on the surface of the hydrogel in the 10% NC group than that in the other two groups (Fig. 1f and Supplementary Fig. S3). *In vivo* degradation experiments demonstrated that the degradation rate of the 10% NC group was the slowest (10% NC: $7.8 \pm 0.01\%$ versus 5% NC: $14.6 \pm 0.01\%$, 0% NC: $28.3 \pm 0.01\%$, $p < 0.05$) *in vivo* total degradation after 28 days (Supplementary Fig. S4). We chose 10% NC as the optimal formula in making extravascular stents for the follow-up experiments.

3.2. Biocompatibility of the NC-Gelatin hydrogel external stent

As shown in Fig. 2a, we have demonstrated the biocompatibility of the stent, including biocompatibility *in vivo* and *in vitro* experiments. The results of the Comet experiment showed that HUVEC cells with the stent do not cause DNA damage in the cells (Fig. 2b and d and Supplementary Fig. S5). The CCK-8 assay revealed no differences in cell viability after 24, 48, and 72 h of culture with the stent (Fig. 2c). Furthermore, HUVECs cultured with stents were labeled using a Live/dead cell kit, and the results showed that most HUVECs grew well (Fig. 2e).

For the locally embedded site of the stent, macrophages infiltrated after 3 days of embedding, and the number of CD68, CD206, and iNOS positive cells increased, however the number of positive cells gradually decreased on day seven and there was no marked difference between the control and stent groups indicating that the stent has good local tissue biocompatibility (Fig. 3a and b, Supplementary Figs. S6, S7, S8, S9, and S10). To evaluate the damage of the stent to important organs of the body, we performed H&E and Masson staining of the heart, liver, spleen, lung, and kidney; no obvious morphological changes were found 3 and 7 days after the operation (Fig. 3c, Supplementary Figs. S11, S12, and S13). No obvious changes in various cell components were shown according to flow cytometry analysis of blood samples taken after 3 and 7 days (Fig. 3d and e, Supplementary Fig. S14). In comparison of both stents, ELISA for pro-inflammatory and anti-inflammatory cytokines in the blood after 3 and 7 days showed no obvious changes (Supplementary Figs. S15 and S18). No obvious changes in various cell components could be seen from the flow cytometry analysis of spleen samples taken after 3 and 7 days (Supplementary Figs. S16 and S19). Furthermore, according to the RT-PCR analysis of the spleen cells, there were no obvious differences in the expression levels of pro-inflammatory and anti-inflammatory indicators between days 3–7 (Supplementary Figs. S17 and S20).

3.3. The NC-Gelatin stent inhibits restenosis by resisting EndMT through the autophagy pathway

As shown in Fig. 4a, we established a rat autologous jugular vein-carotid artery graft vein model and included a stent. Four weeks later, we performed Color Doppler Ultrasound on the rats to evaluate the condition of the vein grafts. We found that arterial flow was faster than venous flow, causing the velocity of narrow vein graft vessels to increase. Following the stent intervention, the flow rate decreased in the vein graft, increasing the patency rate significantly (Stent: 141 ± 1.4 cm/s versus Graft: 166 ± 5.9 cm/s, Arterial flow: 88 ± 5.3 cm/s, Venous flow: 14 ± 1.4 cm/s, $p < 0.05$; Fig. 4b and c). We performed H&E and Masson staining (Fig. 4d and Supplementary Fig. S21) on the specimens four weeks after the operation; the stent significantly reduced intimal hyperplasia as the intimal thickness of the stent group was significantly lower than the graft group (Stent: $445.3 \mu\text{m} \pm 150.0$ versus Graft: $676.4 \pm 204.7 \mu\text{m}$, Artery: $48.9 \pm 8.2 \mu\text{m}$, Vein: $11.7 \pm 2.9 \mu\text{m}$, $p < 0.05$; Fig. 4e), and the wall thickness of the stent group was also significantly reduced (Stent: $570.0 \pm 153.5 \mu\text{m}$ versus Graft: $786.0 \pm 210.6 \mu\text{m}$, Artery: $48.9 \pm 8.2 \mu\text{m}$, Vein: $34.6 \pm 9.7 \mu\text{m}$, $p < 0.05$; Fig. 4f). The stent significantly reduced the intimal/vessel wall ratio (Stent: 0.77 ± 0.08 versus Graft: 0.86 ± 0.06 , Artery: 0.50 ± 0.08 , Vein: 0.36 ± 0.14 , $p <$

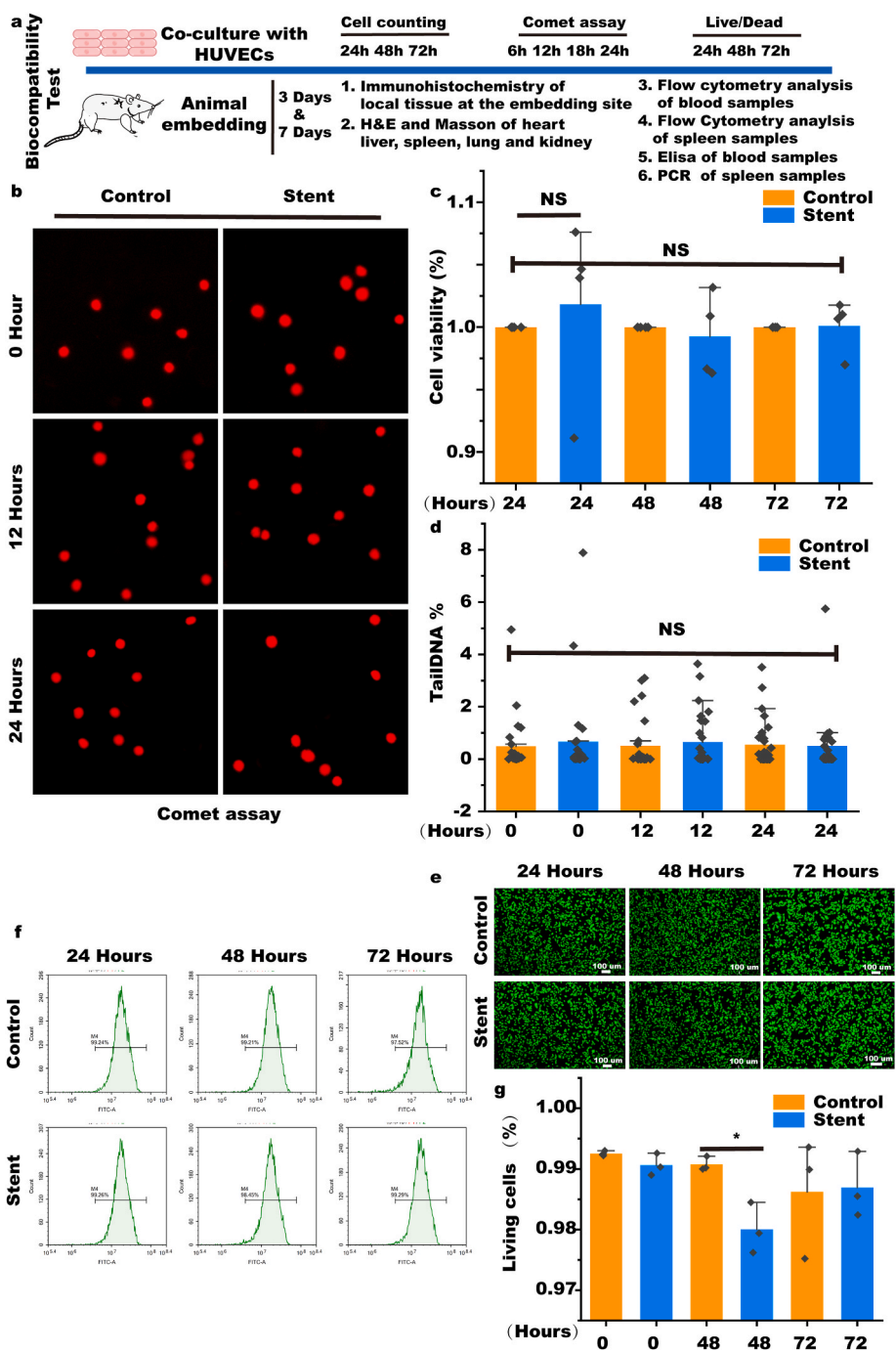


Fig. 2. *In vitro* biocompatibility evaluation of the stent. (a) Schematic diagram of the systematic biocompatibility evaluation of NC-hydrogels. (b & d) Comet assay to assess DNA damage by the stent. (c) Cell viability assay of cells cultured with stent (n = 4). (e, f & g) Biocompatibility evaluation based on the Live/dead staining (n = 3). Data are expressed as means ± standard deviations (n = 3); NS indicates not significant.

0.05; Fig. 4f). We also measured the area of the intima and found that area in the stent group was significantly lower than that in the graft group (Stent: $1.97 \pm 0.74 \text{ mm}^2$ versus Graft: $2.53 \pm 1.45 \text{ mm}^2$, Artery: $0.10 \pm 0.01 \text{ mm}^2$, Vein: $0.05 \pm 0.02 \text{ mm}^2$, $p < 0.05$), and the intimal/lumen area ratio was also the lowest in the stent group (Stent: 0.59 ± 0.06 versus Graft: 0.71 ± 0.07 , Artery: 0.25 ± 0.03 , Vein: 0.22 ± 0.08 , $p < 0.05$; Fig. 4f). We conducted α -SMA and CD31 fluorescent double staining on the grafted veins and found that both α -SMA and CD31 were co-expressed in the graft group, revealing the process of EndMT. The expression of α -SMA in the stent group was lower, suggesting that the stent inhibited the process of EndMT in the grafted veins (Fig. 4g). To verify that the stent could resist EndMT, we performed Western blot and

RT-PCR detection on the vein grafts; the stent remarkably increased the expression of CD31 in the grafted veins, whereas it considerably decreased the expression of α -SMA (Supplementary Figs. S22a and b). The stent also markedly reduced the expression of slug, snail, twist, and vimentin, which are hallmarks of EndMT in the grafted veins (Supplementary Fig. S22a & b). We found that the stent reduced the expression of IL-1 β , which is key to the induction of EndMT (Supplementary Fig. S22c).

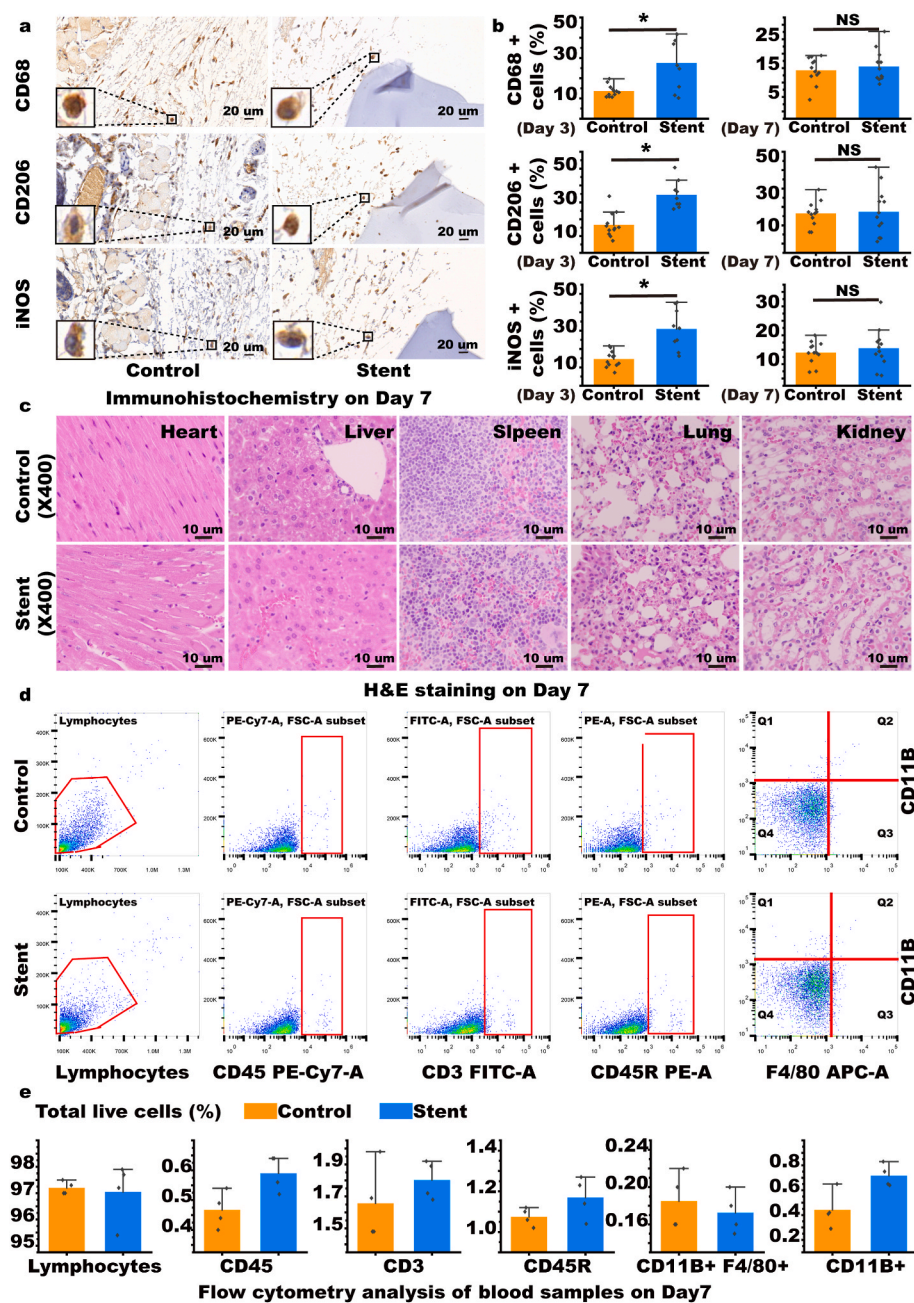


Fig. 3. Evaluation of *in vivo* biocompatibility. (a & b) Immunohistochemistry of CD68, CD206, and iNOS in local tissues of mice with embedded stent to assess macrophage infiltration. (n = 9). (c) Hematoxylin and eosin (H&E) staining of the heart, liver, spleen, lung, and kidney of mice with embedded stent to assess systemic toxicity. (d & e) Flow cytometry of blood from mice with the embedded stent to assess systemic inflammatory responses (n = 4). Data are expressed as means ± standard deviations (n = 3); NS indicates not significant; *p < 0.05.

3.4. The external stent loaded with AS-IV resists EndMT by activating autophagy

The mechanism by which the stent reduced key inflammatory factors, including IL-1 β which induces EndMT, was investigated *in vitro* [37, 38]. A typical characteristic of EndMT in endothelial cells is the decrease of CD31 and the increase of α -SMA, twist, snail, and slug (Fig. 5a). Based on the results of fluorescent double staining, a high concentration (15 ng/mL) of IL-1 β reduced CD31 expression considerably and increased α -SMA expression considerably compared with a low concentration of 5 ng/mL. Furthermore, cells in the high-dose group compared with the low-dose group became slenderer, showing a more typical EndMT cell morphology (Fig. 5b and Supplementary Fig. S23). Inhibiting the expression of IL-1 can activate autophagy. Moreover, autophagy level also changes markedly with the occurrence and development of EndMT, suggesting that autophagy mediates EndMT [39,40]. We found that along with the increase in EndMT marker proteins including slug, snail,

and twist, autophagy-specific proteins such as beclin 1 and LC3 decreased, with the RT-PCR results confirming these findings, therefore suggesting that autophagy mediates EndMT (Fig. 5c, d, & e and Supplementary Fig. S24). Using TEM (Transmission Electron Microscopy, TEM), we observed that when exposed to the high dose of IL-1 β , the contents of the autophagosome and autophagolysosomes in EndMT cells were less than when exposed to the low dose of IL-1 β (Fig. 5f).

We used the drug AS-IV and found that it inhibited EndMT more strongly compared with the absence of the drug and that a higher concentration of the drug AS-IV inhibited more EndMT than when used at lower concentrations (Fig. 6a). To explore whether AS-IV inhibits the EndMT process through the autophagy pathway, we double-stained twist and LC3 and found that AS-IV reduced the expression of twist and increased the expression of LC3; thus, the high-dose was proven more effective than the low-dose (Fig. 6b). The results of Western blot and RT-PCR also found that AS-IV could activate autophagy and that the expression of LC3, CD31, and beclin was increased; the expression of

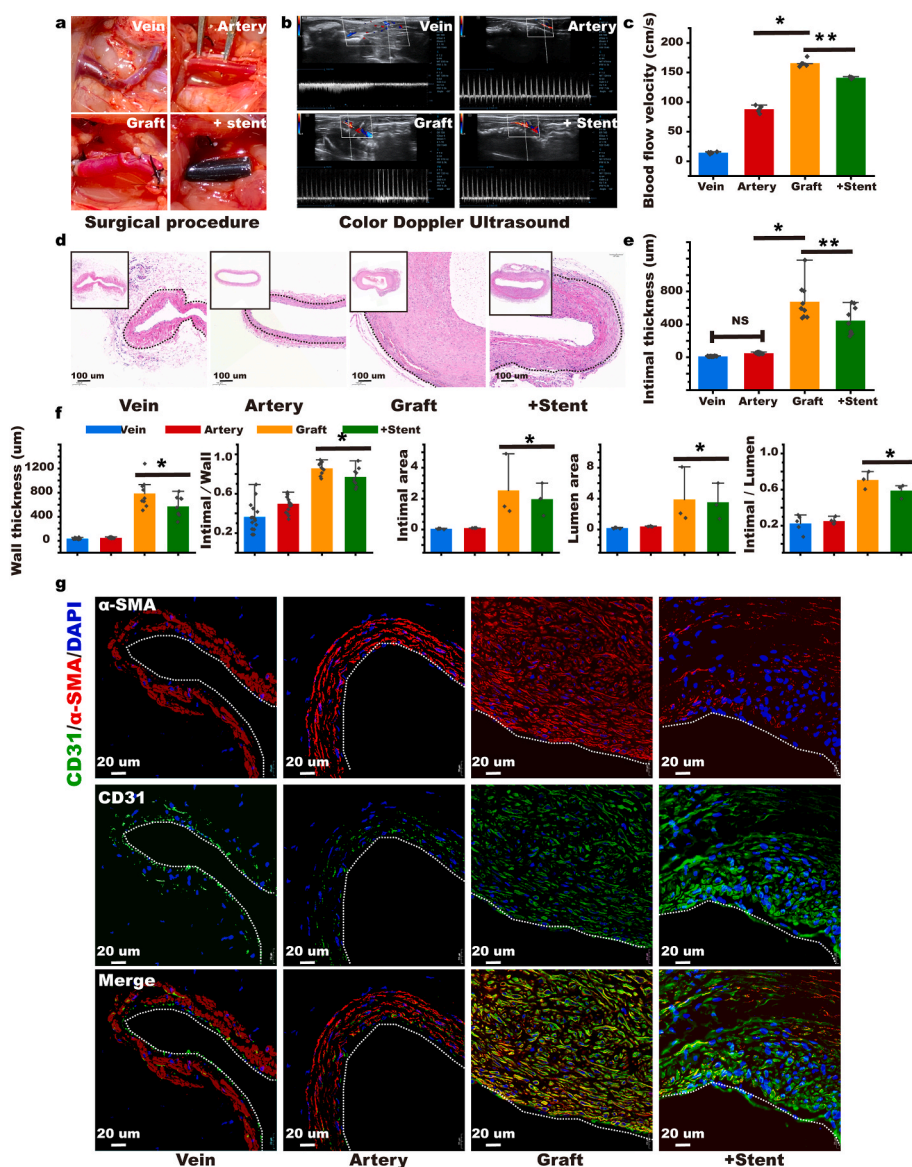


Fig. 4. Stent inhibits graft vein restenosis by resisting endothelial-to-mesenchymal transition (EndMT). (a) Establishment of a rat autografted vein model and intervention with stent. (b & c) Four weeks after the model was established, Color Doppler ultrasonography was used to detect the blood flow in the graft vein to evaluate restenosis. (n = 5). (d) H&E was performed 4 weeks after the vein was grafted to observe intimal hyperplasia (the black dotted line indicates the interval between intima and adventitia). (e & f) Statistics of the main indicators of intimal hyperplasia. (n = 5). (g) α -SMA and CD31 immunofluorescence double staining was performed 4 weeks after the transplanted vein to evaluate the resistance of stent to EndMT (the white dotted line indicates the interval between the lumen and intima) (n = 5). Intimal thickness refers to the thickness of the intima. Wall thickness refers to the thickness of the grafted vein. Intimal/wall refers to the proportion of intimal thickness in the grafted vein. Intimal area refers to the area of the intima in this cross section. The lumen area is the area of the graft vein in this cross-section. Intimal/lumen refers to the proportion of the intimal area to the grafted vein area in this cross-section. Data are expressed as means \pm standard deviations (n = 3); NS indicates not significant; * p < 0.05.

p62, α -SMA, slug, twist, and snail was decreased showing EndMT inhibition (Fig. 6c, d, & e and Supplementary Fig. S25). Using TEM, after treatment with AS-IV, the contents of autophagosome and autophagolysosomes increased. This was proven to be dose dependent (Fig. 6f).

3.5. NC-Gelatin-AS-IV external stent inhibits graft restenosis and resists EndMT by activating autophagy

We hypothesized a stent loaded with AS-IV could synergistically enhance the effect of stent-activated autophagy against EndMT; therefore, we prepared an NC-Gelatin-AS-IV loaded stent. FTIR was used to observe the absorption peak of the hydroxyl stretching vibration at 3390 cm^{-1} (Fig. 7a). Overall drug release was smooth and the cumulative amount of release in 30 days was approximately $47 \pm 0.01\%$ (Fig. 7b). The advantage of administering medication locally is that the target tissue can be affected with few systemic side effects. We measured the AS-IV concentration in the blood and found no trace of the drug in the test samples, which follows our hypothesis (Supplementary Figs. S26 and S27). In addition, we used a bare stent and different concentrations of AS-IV-loaded stent in rat vein graft surgeries. We found that the drug-loaded AS-IV-stent could improve the patency rate of the grafted veins and its effect would be enhanced at a high concentration (Fig. 7c and d).

We performed H&E and Masson staining on vein grafts to assess intimal hyperplasia and found that AS-IV enhanced the effect of the stent in reducing intimal thickness. Furthermore, the effect was enhanced at higher concentrations of the drug (High: $171.7 \pm 67.0\ \mu\text{m}$ versus Low: $253.8 \pm 68.7\ \mu\text{m}$, Stent: $445.3 \pm 150.0\ \mu\text{m}$, Graft: $676.4 \pm 204.7\ \mu\text{m}$, $p < 0.05$). The intimal/wall thickness ratio showed concurring results (High: 0.498 ± 0.121 versus Low: 0.680 ± 0.070 , Stent: 0.770 ± 0.084 , Graft: 0.857 ± 0.060 , $p < 0.05$). In addition, the two indicators of the intimal area and the ratio of the intimal area/lumen area in the high dose group were the most effective (Intimal area: High: $0.65 \pm 0.24\ \text{mm}^2$ versus Low: $0.97 \pm 0.36\ \text{mm}^2$, Stent: $1.97 \pm 0.74\ \text{mm}^2$, Graft: $2.53 \pm 1.45\ \text{mm}^2$, $p < 0.05$; Intimal/lumen: High: 0.31 ± 0.03 versus Low: 0.51 ± 0.13 , Stent: 0.59 ± 0.06 , Graft: $0.71 \pm 0.07\ \text{mm}^2$, $p < 0.05$; Fig. 7d and e and Supplementary Fig. S28d).

We performed double fluorescent staining of CD31 and α -SMA on the grafted vein and found that they were co-expressed in the graft group, which represented the occurrence of EndMT. Stent intervention could increase CD31 expression and reduce the expression of α -SMA, inhibiting EndMT; this effect was enhanced at high doses of AS-IV (Fig. 8a). Based on our findings, we suggest that AS-IV can improve EndMT stent resistance in the grafted vein (Fig. 8b and c and Supplementary Fig. S29). To explore whether autophagy is involved in the resistance

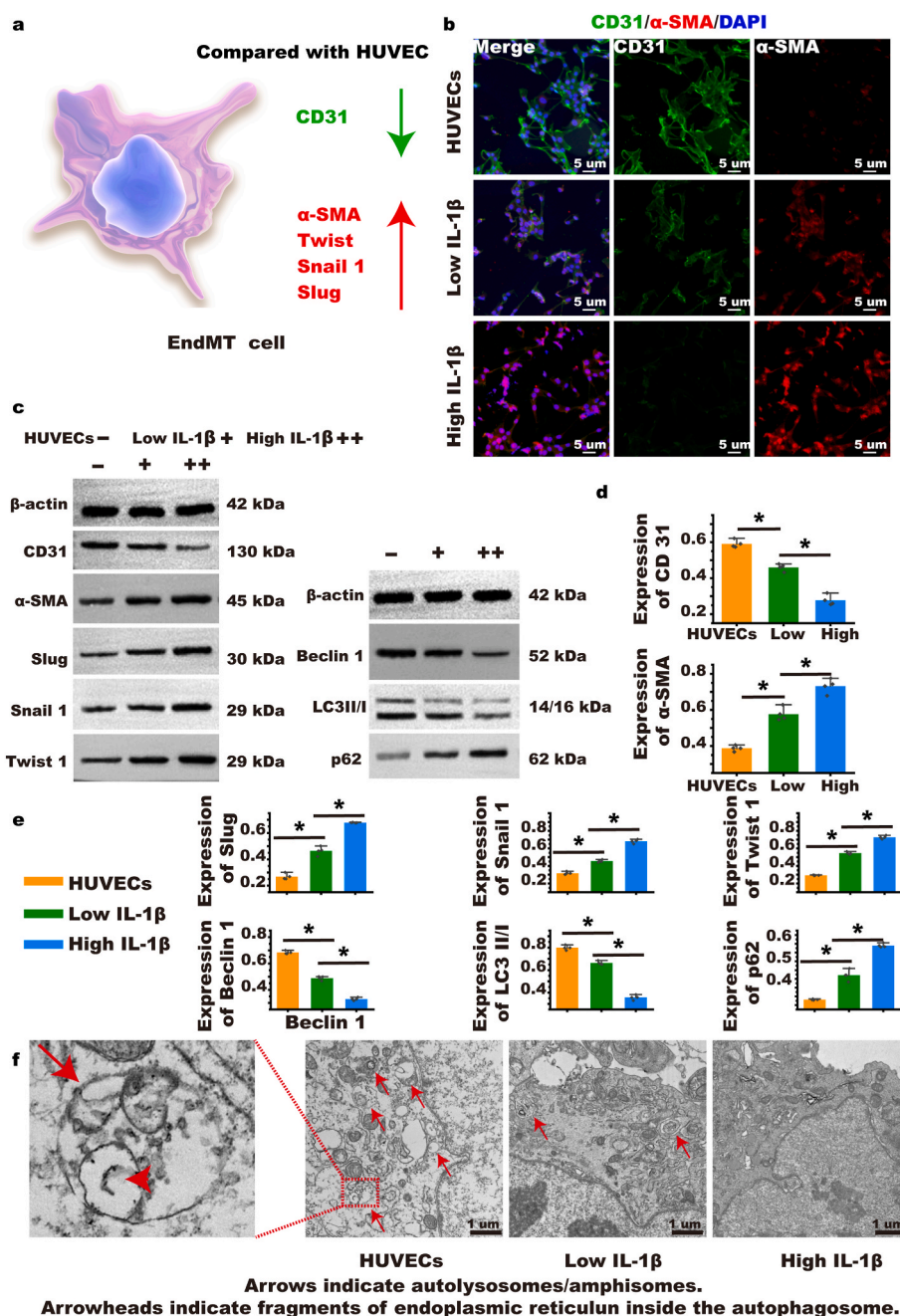


Fig. 5. EndMT changes in human umbilical vein endothelial cells (HUVECs). (a) Mechanism of EndMT in HUVEC. (b) After EndMT induction by high and low concentrations of IL-1β, double staining was used for identification of α-SMA and CD31. (c, d, & e) The induced EndMT cells were collected, and Western blot was used to detect EndMT characteristic proteins and autophagy-related proteins. (n = 4). (f) Transmission electron microscopy (TEM) was used to observe the autophagosome and autolysosome of EndMT under different conditions. (n = 4). Group explanation: HUVECs refer to uninduced HUVECs, low IL-1β indicates that a low-dose IL-1β induces EndMT in HUVECs, and high-IL-1β indicates that a high-dose IL-1β induces more obvious EndMT in HUVECs. Data are expressed as means ± standard deviations (n = 3); *p < 0.05.

process of EndMT, we performed fluorescent double staining of autophagy core protein LC3 and EndMT core protein twist on grafted veins. In the graft group, the expression of twist was high, while that of LC3 was low. This indicated that autophagy was significantly inhibited during EndMT. In the presence of the stent, the expression of LC3 increased and the expression of twist decreased, indicating that the autophagy pathway is activated to inhibit EndMT. With a stent loaded with AS-IV, autophagy was further activated and EndMT was further inhibited, indicating that AS-IV can strengthen the activation of autophagy. This effect was also found to be dose dependent, so a high dose of AS-IV was more effective in inhibiting EndMT than a low dose of the drug (Fig. 8d). We detected the protein and mRNA of twist, LC3, p62, and Beclin by Western blot and RT-PCR (Fig. 8e and f and Supplementary Fig. S29). Thus, we suggest that the NC-Gelatin-AS-IV loaded extravascular stent resists EndMT by activating autophagy and inhibiting graft restenosis.

4. Discussion

In this study, we prepared an extravascular NC-Gelatin stent loaded with AS-IV. We found that the stent has good physicochemical properties and biocompatibility, as shown *in vivo* and *in vitro*. Furthermore, the stent could activate the autophagy pathway, resist EndMT in the grafted vein, and prevent restenosis. Moreover, the addition of the drug AS-IV could enhance these effects *in vivo* and *in vitro*. These findings are beneficial in revealing the mechanism of extravascular stent in reducing restenosis and provide options for the design and application of extravascular stent. Our results provide novel ideas and methods for the clinical application of an extravascular stent to improve restenosis of grafted veins.

The NC-Gelatin extravascular stent has suitable physicochemical properties to prevent restenosis of the grafted veins. Grafted veins are widely used for revascularization, but restenosis affects patient quality

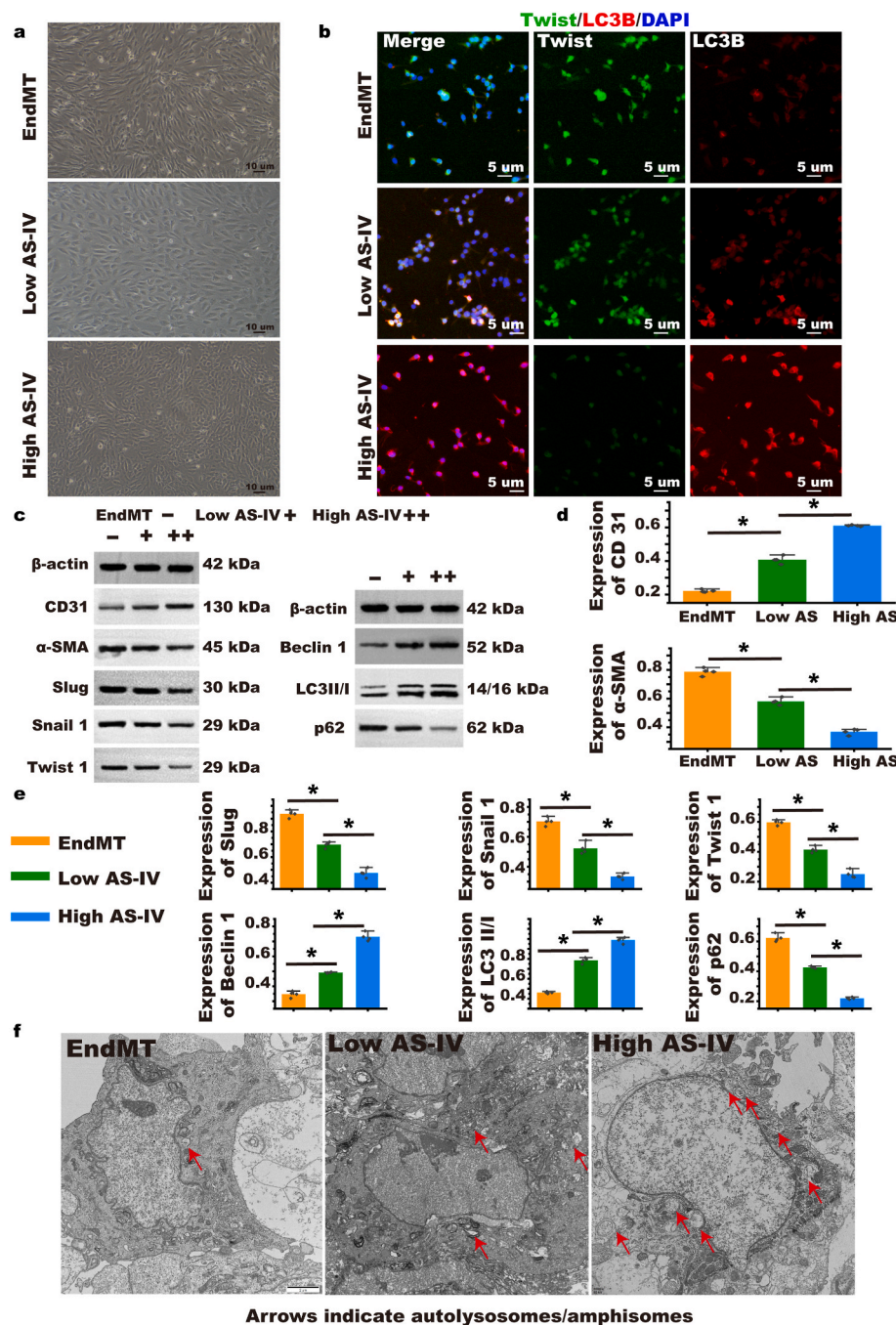


Fig. 6. EndMT was inhibited by Astragaloside IV (AS-IV), and changes in autophagy and EndMT were observed. (a) Morphological changes of EndMT cells after AS-IV intervention were observed in a bright field. (b) EndMT cells after AS-IV intervention were double stained with EndMT characteristic protein twist and the autophagy characteristic protein LC3B. (c, d, & e) In EndMT cells after AS-IV intervention, Western blot was used to detect EndMT characteristic proteins and autophagy-related proteins. (n = 4). (f) After AS-IV intervention in EndMT cells, TEM was used to evaluate the contents of autophagosome and autophagolysosomes in different groups. Group explanation: EndMT refers to the change of EndMT in HUVECs induced by high-dose IL-1β, low AS-IV refers to EndMT cells intervened with low-dose AS-IV, high AS-IV refers to EndMT cells intervened with high-dose AS-IV. Data are expressed as means ± standard deviations (n = 3); *p < 0.05.

of life and long-term prognosis. Recently, extravascular stents have been used to buffer the high pressure experienced by vein grafts and their subsequent vasodilation, reduce endothelial damage and inflammation, and prevent restenosis [41–43]. The process of grafting vein surgery causes damage to the endothelium. Thus, during operations, the "NO-TOUCH" principle should be followed to prevent stenosis [44]. Within a few hours after the grafting of the vein, the lumen surface gets covered with rich fibrin. After which, the white blood cells in the circulating blood, including neutrophils, monocytes, and lymphocytes, attach to the intima, causing thrombosis requiring intensive anticoagulation therapy, such as with heparin and aspirin [45]. After a few days, the grafted vein releases growth factors and cytokines, such as inflammatory cells, that promote endothelial cell EndMT and smooth muscle cell proliferation. This phase often lasts about a year and can be intervened with extravascular stents [46]. Approximately 2 years later,

macrophages on the vascular wall begin to ingest adipocytes and transform into dead foam cells undergoing apoptosis and eventually depositing cholesterol to form necrotic nuclei. At this stage, anti-atherosclerotic therapy, e.g., with atorvastatin, is often effective [47]. Extravascular stents can be divided into either solid or semi-solid according to their shape. The representative of semi-solid stents is gel and its biggest advantage is its ease of use. The main concerns of scholars on this gel focus on its mechanical properties. However, this can be easily tweaked through modification of its materials [48]. Solid type extravascular stents, including mesh, sheath, cuff, wrap, and matrix, can often provide enough support. As a result, these stents are not particularly easy to use, especially for coronary artery bypass graft [46]. Drug-loaded stents, with drug-loaded coatings inside the stent or a polymer, are now favored over bare stents. Among commercial stents, sirolimus is the most encapsulated drug, and its release rate is reported

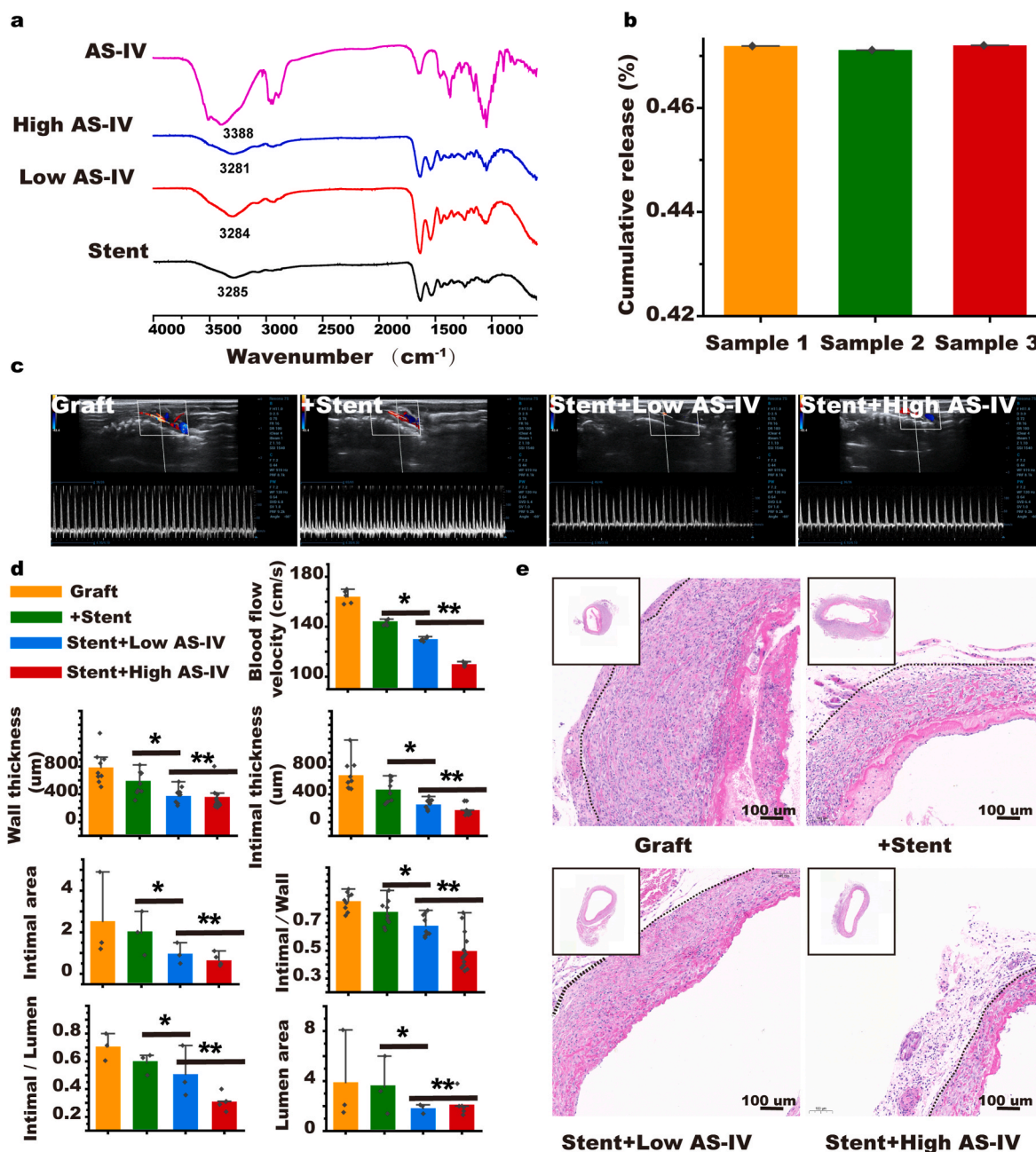


Fig. 7. NC-hydrogel extrinsic stent-encapsulated with AS-IV. (a) FT-IR identification of the stent packaged with AS-IV. (b) *In vitro* cumulative release rate. (c) Evaluation of patency rate 4 weeks after stent embedding and AS-IV loaded stent with different doses of AS-IV. (d & e) H&E staining performed 4 weeks after embedding of the stent and AS-IV-loaded stent with different doses of AS-IV to evaluate intimal hyperplasia (the black dotted line indicates the interval between the intima and adventitia). (n = 5). Data are expressed as means ± standard deviations (n = 3); **p* < 0.05.

to be generally maintained at 30%–70%. The significant advantage of drug-loaded stents is that the drug can effectively reach the target tissue, resulting only in a few systemic side effects [49]. In order to reduce the side effects caused by permanent stent implantation, biodegradable stents have been developed rapidly in recent years. The research and development of biodegradable stents in the past 20 years has mainly focused on materials such as polymers, iron, magnesium, and zinc. These materials can temporarily support blood vessels for 3–6 months after implantation in the body and then be degraded and absorbed [50]. Once a material is completely degraded, no foreign bodies form around the blood vessels and vascular reactivity with vascular remodeling potential can then be restored.

Extravascular supports, such as gel, mesh, sheath, cuff, warp, matrix, and stent, possess variable advantages and disadvantages. However, the

most important aspect to consider is the support provided to the grafted vein [46]. We chose the reaction of gelatin and genipin as the basis for fabricating an extravascular stent and adjusted the mechanical properties of the stent by adding different ratios of NC. The pure gelatin hydrogel has a porous morphology with connected pores, and the wall surface of the pores is relatively smooth. Nanocellulose can be adsorbed on the surface of hydrogel wall material through hydrogen bonding and hydrophobic interaction to form a dense network structure. The high-density network structure can effectively enhance the expansion strength of gelatin hydrogel and improve the application performance of the hydrogel. The *in vitro* expansion experiment indicated that the effects of the graft vein expansion inhibition were optimal. NC-hydrogel is a highly hydrated porous fibrous and soft material with good mechanical properties; it can be chemically modified by adding functional

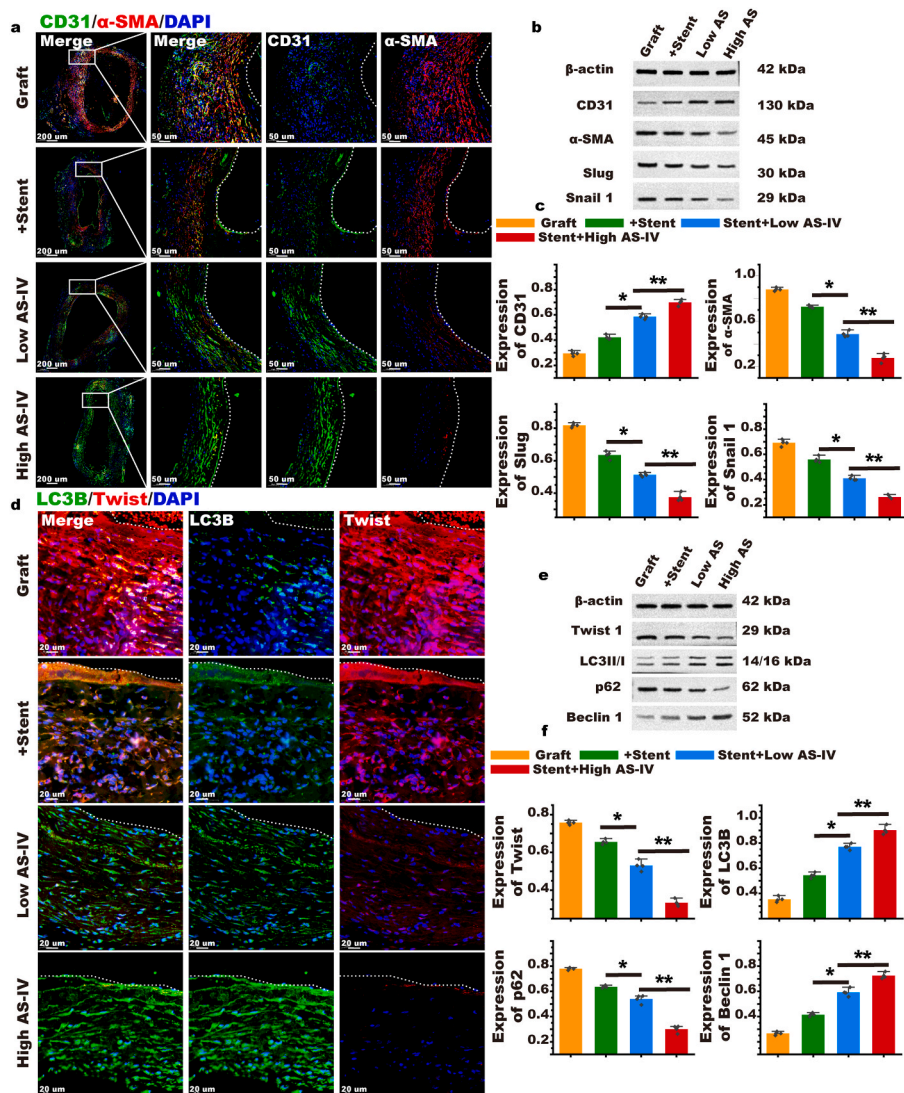


Fig. 8. AS-IV could enhance the effect of the stent to activate autophagy against EndMT. (a) α -SMA and CD31 immunofluorescence double staining were performed 4 weeks after the vein was transplanted to evaluate the effect of AS-IV on enhancing the stent's resistance to EndMT (the white dotted line indicates the interval between the lumen and the intima). (b & c) Western blot detection of the EndMT core protein to evaluate the effect of AS-IV in enhancing the resistance of the stent to EndMT. (d) Twist and LC3B fluorescent double staining was performed on the grafted vein to evaluate the effect of AS-IV on enhancing the resistance of the stent to EndMT through autophagy (the white dotted line indicates the interval between the lumen and intima). (e & f) Western blot was used to detect the core protein of autophagy and EndMT and to evaluate the effect of AS-IV on enhancing the resistance of the stent to EndMT through autophagy. (n = 5). Data are expressed as means \pm standard deviations (n = 3); * p < 0.05.

groups or grafted biomolecules that can enhance the physicochemical properties and biological interactions of hydrogels. Moreover, NC-hydrogels have been suitable for biomedical applications [51–54]. Prakobna and Kasinee reported that adding NC to the hydrogel can improve Young's modulus by a factor of 7, and Yang et al. reported that the mechanical properties can be improved by a factor of 8.5 [55,56]. NC-hydrogel is widely used in tissue engineering, such as 3D cell culture and bone defects. We innovatively applied it to extravascular stents to prevent restenosis of grafted veins, which has broadened its application [57–61]. Markstedt et al. 3D printed NC-hydrogels followed by cell culture for the reconstruction of human ear cartilage and achieved positive results; the success of this study was based on the excellent viscosity of NC-hydrogels, shear thinness, and low shear rates for good 3D printing performance [62–66]. Our study took full advantage of the excellent mechanical properties of NC-hydrogels to limit the dilation of the grafted vein under high pressure, alleviate intimal hyperplasia, and prevent restenosis.

The NC-Gelatin extravascular stent has excellent biocompatibility, which is critical for grafting veins [67–69]. An important characteristic to consider when designing an extravascular stent is to ensure that it limits the inflammatory response, thus resisting EndMT and inhibiting the grafted vein stenosis. We conducted a systematic local biocompatibility investigation and found that the number of macrophages increased slightly after 3 days, which could have been caused by an

acute reaction. However, after 7 days, the number of macrophages was similar to that of the control group, showing good biocompatibility. This interesting result is attributed to the excellent biocompatibility of NC-hydrogels. Hydrogels and NC are biocompatible. Their synthesis requires a washing step to remove potentially harmful cells and tissues [70–72]. If necessary, UV irradiation and ozone can sterilize hydrogels after preparation to minimize contamination by microorganisms such as bacteria and fungi [73,74]. To date, no significant toxic effects of NC on cells and organs have been reported [75]. A similar antibacterial effect was found in an NC-hydrogel as a wound dressing [76,77]. We evaluated the cytotoxicity of NC-hydrogels and found no cytotoxicity of the fabricated NC-Gelatin hydrogel. NC-hydrogels are used for the 3D culture of mesenchymal stem cells, human pluripotent stem cells, and liver tumor cells [78–81]. In this study, we evaluated the pathological conditions of the heart, liver, spleen, lung, and kidney of rats after embedding the stent and evaluated the systemic inflammatory response as follows: blood and flow cytometry of the spleen, ELISA of inflammation-related components of blood, and RT-PCR of spleen contents [82,83]. This systematic biocompatibility evaluation lays a solid foundation for later clinical use of the extravascular stent.

External stents prevent restenosis by activating autophagy against EndMT. Using cell lineage tracing technology, scholars found that EndMT was mediated by the sudden increase in pressure after the grafted vein was exposed to the arterial system, and over 50% of the

neointima were EndMT cells; postmortem autopsy in patients who had undergone vein grafting revealed that EndMT cells were the major component of the neointima [84–86]. Inflammation has always been associated with restenosis and intimal hyperplasia. Professor Fumitaka Ohsuzu reported that IL-6 is involved in intimal hyperplasia after vascular injury. The mechanism includes I κ BNS regulation of a subset of Toll-like receptor (TLR)-dependent genes including interleukin –6 (IL-6) by inhibiting nuclear factor- κ B (NF- κ B) [87]. Prof. David Bernhard reported that IL-8 is involved in intimal hyperplasia, and its mechanism includes Endothelial cell-secreted interleukin 8 triggering intimal invasion of smooth muscle cells and enhancing intimal thickening in an arterial organ culture model [88]. NF- κ B signaling is widely involved in remodeling after vasculitic infiltration. Prof. Hideki Katagiri found that Endothelial NF- κ B activation up-regulates adhesion molecule expression, which may trigger macrophage infiltration and inflammation in the adventitia and media. Thus, the endothelium plays an important role in vascular remodeling through its intracellular NF- κ B signaling [89]. Prof. Garret A Fitzgerald found that COX-2-derived prostacyclin modulates vascular remodeling. Among which, deletion of the PGI₂ receptor (IP) or suppression of PGI₂ with the selective COX-2 inhibitor, nimesulide, both augmented intimal hyperplasia while preserving luminal geometry in mouse models of transplant arteriosclerosis or flow-induced vascular remodeling [90]. Our study found that the NC-hydrogel extravascular stent can limit the dilatation of the graft vein and resist EndMT, thus preventing restenosis. *In vivo* and *in vitro* experiments showed extravascular stents resist EndMT by activating autophagy. Inhibition of IL-1 β can activate autophagy. Changes in autophagy levels affect EndMT. In this study, we found that our fabricated stent reduces IL-1 β by limiting expansion, thus activating autophagy and resisting EndMT [39,40,91]. This finding helps elucidate the mechanism of extravascular stents to prevent restenosis of grafted veins as well as helps select drugs loaded with extravascular stents.

AS-IV can enhance the effect of the stent to activate autophagy against EndMT. AS-IV is a saponin purified from *Astragalus*, a traditional Chinese herbal medicine widely used for cardiovascular and cancer treatment for over 2000 years [92]. Xu et al. reported that AS-IV may down-regulate mRNA expression of IL-1 β , IL-6, and TNF- α , all of which induce EndMT [93]. Xiong et al. reported that AS-IV reduced mRNA expression levels of NLRP3, IL-1 β , IL-18, IL-6, TNF- α , and IL-8 and demonstrated the anti-inflammatory functions of AS-IV. Furthermore, they found that AS-IV can promote autophagy [31]. In this study, we found that AS-IV can inhibit IL-1 β -induced EndMT, in which autophagy is significantly activated, and the effect of a high dose of the drug is better than that of a low dose. To reduce systemic adverse reactions and improve the local effect, we loaded AS-IV into the stent and proved the feasibility of locally applying AS-IV through *in vitro* release experiments and *in vivo* blood concentration detection. Gao et al. reported the local application of AS-IV to induce wound healing and found that AS-IV has a good anti-inflammatory effect [94]. We found through a rat graft vein model that adding AS-IV can enhance the effect of the stent to activate autophagy against EndMT and is dose dependent. Simultaneously, we demonstrated the safety and efficacy of AS-IV. First, the advantage of local tissue targeting with few systemic side effects is achieved [95]. Local application of AS-IV around the graft vein in the current study was based on this principle; we aimed to reduce the systemic toxicity of AS-IV while exerting local effects. Our animal experiments illustrated the effectiveness of AS-IV, and in order to quantitatively analyze the contents of AS-IV in the blood, we performed blood concentration analyses. Second, low plasma concentration of topical drugs, leading to false-negative results, were of concern. Therefore, we emphasized great importance to the establishment of a standard curve in order to improve the test efficiency. The precision of our standard curve was chosen to be in ng/mL, which is sufficient to detect trace amounts of AS-IV in blood, thereby avoiding false negatives. Establishment of the standard curve is shown in [Supplementary Fig. S26](#). The results demonstrated that none of the AS-IV in the test samples was detected in blood. Combined with the

experiments described above, these results suggested that topical AS-IV was safe. Furthermore, *in vitro* experiments demonstrated that AS-IV blocked intimal hyperplasia. In conclusion, topical application of AS-IV to inhibit restenosis of graft vein proved safe and effective. These results may help optimize the use of extravascular stents in clinical treatment.

There are limitations to this study. First, the animal model pathophysiology of vein grafts does not adequately mimic the complexity of human coronary artery bypass grafting. Second, all interventions were conducted in healthy animals; however, various chronic comorbidities can usually be found clinically in a patient. Therefore, studies that consider these factors are needed for further practical applications.

5. Conclusions

NC-Gelatin extravascular stents can activate autophagy, resist EndMT, and prevent restenosis of graft vein. Furthermore, these effects can be significantly enhanced when AS-IV is loaded on the stent. We have demonstrated the effectiveness of our fabricated extravascular stent using NC-Gelatin loaded with the AS-IV drug. We have shown that restenosis can be prevented in vein grafts with these extravascular stents. This is done through the inhibition of the inflammatory process leading to EndMT, thereby reducing the chance of vein graft failure.

Authorship contribution statement

Tianshu-Chu: conceptualization, methodology, resources, writing-original draft. Qingye-Li: methodology. Chun-Dai: visualization, supervision. Xiang-Li: supervision. Xiang-Kong: visualization, supervision. Yangming-Fan: visualization, supervision. Hongyan-Yin: visualization. Jianjun-Ge: conceptualization, project administration, funding acquisition.

Ethics approval

In expansion analysis, all procedures were performed under the Declaration of Helsinki of ethical standards of the 1964 and the First Affiliated Hospital of USTC (committee approved, Ethics No. 2021KY Ethical No. 51).

All animal procedures obtained approval from the Ethics Committee of USTC (Ethics number: 2019-N(A)-086) and met the requirements of the National Institutes of Health Guide for the Care and Use of Laboratory Animals (NIH Publications No. 8023, revised 1978).

Consent to participate

We gained the informed consent for using human subjects in the study. Privacy rights of human subjects were respected throughout.

Statement of informed consent

We have obtained informed consent for this experimentation with human subjects. The privacy rights of human subjects must always be observed.

Data availability

All data supporting the findings of this study are available within the article and its Supplementary Information files, or are available from the corresponding authors upon reasonable request.

Informed consent statement

We gained the informed consent for using human subjects in the study. Privacy rights of human subjects were respected throughout.

Funding

This work gained supports by the Natural Science Foundation of Anhui Province (Grant No. 2008085MH240), the Major Science and Technology Project of Anhui Province (Grant No. 18030801132), and the R&D projects for medical and health institutions of Hefei (Grant No. 2021YL002).

Declaration of competing interest

The authors declare that they have no known competing financial interests or personal relationships that could have appeared to influence the work reported in this paper.

Acknowledgements

The authors would like to thank XR Huang for their assistance with the study, and we would like to thank Editage (www.editage.cn) for their English language editing services.

Appendix A. Supplementary data

Supplementary data to this article can be found online at <https://doi.org/10.1016/j.bioactmat.2022.10.013>.

References

- Caliskan, D.R. de Souza, A. Böning, O.J. Liakopoulos, Y.H. Choi, J. Pepper, C. M. Gibson, L.P. Perrault, R.K. Wolf, K.B. Kim, M.Y. Emmert, Saphenous vein grafts in contemporary coronary artery bypass graft surgery, *Nat. Rev. Cardiol.* 17 (3) (2020) 155–169, <https://doi.org/10.1038/s41569-019-0249-3>.
- Z.Q. Zhang, Y.X. Yang, J.A. Li, R.C. Zeng, S.K. Guan, Advances in coatings on magnesium alloys for cardiovascular stents - a review, *Bioact. Mater.* 6 (12) (2021) 4729–4757, <https://doi.org/10.1016/j.bioactmat.2021.04.044>.
- J.H. Lawson, L.E. Niklason, P. Roy-Chaudhury, Challenges and novel therapies for vascular access in haemodialysis, *Nat. Rev. Nephrol.* 16 (10) (2020) 586–602, <https://doi.org/10.1038/s41581-020-0333-2>.
- M. Hu, F. Jia, W.P. Huang, X. Li, D.F. Hu, J. Wang, K.F. Ren, G.S. Fu, Y.B. Wang, J. Ji, Substrate stiffness differentially impacts autophagy of endothelial cells and smooth muscle cells, *Bioact. Mater.* 6 (5) (2021) 1413–1422, <https://doi.org/10.1016/j.bioactmat.2020.10.013>.
- X. Jiang, M. Shao, X. Liu, X. Liu, X. Zhang, Y. Wang, K. Yin, S. Wang, Y. Hu, P. A. Jose, Z. Zhou, F.J. Xu, Z. Yang, Reversible treatment of pressure overload-induced left ventricular hypertrophy through Drd5 nucleic acid delivery mediated by functional polyaminoglycoside, *Adv. Sci.* 8 (5) (2021), 2003706, <https://doi.org/10.1002/adv.202003706>.
- T. Yamazaki, J.M. Bravo-San Pedro, L. Galluzzi, G. Kroemer, F. Pietrocola, Autophagy in the cancer-immunity dialogue, *Adv. Drug Deliv. Rev.* 169 (2021) 40–50, <https://doi.org/10.1016/j.addr.2020.12.003>.
- R.I. Odle, O. Florey, N.T. Ktistakis, S.J. Cook, CDK1, the other 'master regulator' of autophagy, *Trends Cell Biol.* 31 (2) (2021) 95–107, <https://doi.org/10.1016/j.tcb.2020.11.001>.
- N. Mizushima, B. Levine, Autophagy in human diseases, *N. Engl. J. Med.* 383 (16) (2020) 1564–1576, <https://doi.org/10.1056/NEJMra2022774>.
- T. Chu, C. Dai, X. Li, L. Gao, H. Yin, J. Ge, Extravascular rapamycin film inhibits the endothelial-to-mesenchymal transition through the autophagy pathway to prevent vein graft restenosis, *Biomaterials Advances* 137 (2022), 212836, <https://doi.org/10.1016/j.bioadv.2022.212836>.
- J.C. Kovacic, S. Dimmeler, R.P. Harvey, T. Finkel, E. Aikawa, G. Krenning, A. H. Baker, Endothelial to mesenchymal transition in cardiovascular disease: JACC state-of-the-art review, *J. Am. Coll. Cardiol.* 73 (2) (2019) 190–209, <https://doi.org/10.1016/j.jacc.2018.09.089>.
- J. Bischoff, Endothelial-to-Mesenchymal transition, *Circ. Res.* 124 (8) (2019) 1163–1165, <https://doi.org/10.1161/circresaha.119.314813>.
- S.W. Yi, Y.M. Shin, J.B. Lee, J.Y. Park, D.H. Kim, W. Baek, J.K. Yoon, D.G. Kim, I. S. Shin, C.S. Kim, M.L. Kang, J.W. Yang, H.J. Sung, Dilation-Responsive microshape programming prevents vascular graft stenosis, *Small* 17 (18) (2021), e2007297, <https://doi.org/10.1002/smll.202007297>.
- D.P. Taggart, S. Amin, J. Djordjevic, E.K. Oikonomou, S. Thomas, A.M. Kampoli, N. Sabharwal, C. Antoniadis, G. Krasopoulos, A prospective study of external stenting of saphenous vein grafts to the right coronary artery: the VEST II study, *Eur. J. Cardio. Thorac. Surg.* : official journal of the European Association for Cardio-thoracic Surgery 51 (5) (2017) 952–958, <https://doi.org/10.1093/ejcts/ezw438>.
- D.P. Taggart, Y. Ben Gal, B. Lees, N. Patel, C. Webb, S.M. Rehman, A. Desouza, R. Yadav, F. De Robertis, M. Dalby, A. Banning, K.M. Channon, C. Di Mario, E. Orion, A randomized trial of external stenting for saphenous vein grafts in coronary artery bypass grafting, *Ann. Thorac. Surg.* 99 (6) (2015) 2039–2045, <https://doi.org/10.1016/j.athoracsur.2015.01.060>.
- K.C. Chang, D.J. Lin, Y.R. Wu, C.W. Chang, C.H. Chen, C.L. Ko, W.C. Chen, Characterization of genipin-crosslinked gelatin/hyaluronic acid-based hydrogel membranes and loaded with hinokitiol: in vitro evaluation of antibacterial activity and biocompatibility, *Materials science & engineering, C, Materials for biological applications* 105 (2019), 110074, <https://doi.org/10.1016/j.msec.2019.110074>.
- S. Ilkar Erdagi, F. Asabuwa Ngwabebhoh, U. Yildiz, Genipin crosslinked gelatin-diosgenin-nanocellulose hydrogels for potential wound dressing and healing applications, *Int. J. Biol. Macromol.* 149 (2020) 651–663, <https://doi.org/10.1016/j.ijbiomac.2020.01.279>.
- Y. Han, J. Yang, W. Zhao, H. Wang, Y. Sun, Y. Chen, J. Luo, L. Deng, X. Xu, W. Cui, H. Zhang, Biomimetic injectable hydrogel microspheres with enhanced lubrication and controllable drug release for the treatment of osteoarthritis, *Bioact. Mater.* 6 (10) (2021) 3596–3607, <https://doi.org/10.1016/j.bioactmat.2021.03.022>.
- P. Guan, C. Liu, D. Xie, S. Mao, Y. Ji, Y. Lin, Z. Chen, Q. Wang, L. Fan, Y. Sun, Exosome-loaded extracellular matrix-mimic hydrogel with anti-inflammatory property Facilitates/promotes growth plate injury repair, *Bioact. Mater.* 10 (2022) 145–158, <https://doi.org/10.1016/j.bioactmat.2021.09.010>.
- M.J. Lee, A.E. Sayers, T.M. Drake, P. Singh, M. Bradburn, T.R. Wilson, A. Muruganathan, C.J. Walsh, N.S. Fearnhead, Malnutrition, nutritional interventions and clinical outcomes of patients with acute small bowel obstruction: results from a national, multicentre, prospective audit, *BMJ Open* 9 (7) (2019), e029235, <https://doi.org/10.1136/bmjopen-2019-029235>.
- S. Sharifi, M.M. Islam, H. Sharifi, R. Islam, D. Koza, F. Reyes-Ortega, D. Alba-Molina, P.H. Nilsson, C.H. Dohlman, T.E. Mollnes, J. Chodosh, M. Gonzalez-Andrades, Tuning gelatin-based hydrogel towards bioadhesive ocular tissue engineering applications, *Bioact. Mater.* 6 (11) (2021) 3947–3961, <https://doi.org/10.1016/j.bioactmat.2021.03.042>.
- S.A.A. Ghavimi, E.S. Lungren, T.J. Faulkner, M.A. Josselet, Y. Wu, Y. Sun, F. M. Pfeiffer, C.L. Goldstein, C. Wan, B.D. Utery, Inductive co-crosslinking of cellulose nanocrystal/chitosan hydrogels for the treatment of vertebral compression fractures, *Int. J. Biol. Macromol.* 130 (2019) 88–98, <https://doi.org/10.1016/j.ijbiomac.2019.02.086>.
- J.R. Khurma, D.R. Rohindra, A.V. Nand, Swelling and thermal characteristics of genipin crosslinked chitosan and poly(vinyl pyrrolidone) hydrogels, *Polym. Bull.* 54 (3) (2005) 195–204, <https://doi.org/10.1007/s00289-005-0375-4>.
- X. Xue, Y. Hu, S. Wang, X. Chen, Y. Jiang, J. Su, Fabrication of physical and chemical crosslinked hydrogels for bone tissue engineering, *Bioact. Mater.* 12 (2022) 327–339, <https://doi.org/10.1016/j.bioactmat.2021.10.029>.
- H. Du, W. Liu, M. Zhang, C. Si, X. Zhang, B. Li, Cellulose nanocrystals and cellulose nanofibrils based hydrogels for biomedical applications, *Carbohydr. Polym.* 209 (2019) 130–144, <https://doi.org/10.1016/j.carbpol.2019.01.020>.
- T.V. Patil, D.K. Patel, S.D. Dutta, K. Ganguly, T.S. Santra, K.T. Lim, Nanocellulose, a versatile platform: from the delivery of active molecules to tissue engineering applications, *Bioact. Mater.* 9 (2022) 566–589, <https://doi.org/10.1016/j.bioactmat.2021.07.006>.
- R. Poonguzhali, S.K. Basha, V.S. Kumari, Synthesis and characterization of chitosan-PVP-nanocellulose composites for in-vitro wound dressing application, *Int. J. Biol. Macromol.* 105 (Pt 1) (2017) 111–120, <https://doi.org/10.1016/j.ijbiomac.2017.07.006>.
- A.G. Kurian, R.K. Singh, K.D. Patel, J.H. Lee, H.W. Kim, Multifunctional GelMA platforms with nanomaterials for advanced tissue therapeutics, *Bioact. Mater.* 8 (2022) 267–295, <https://doi.org/10.1016/j.bioactmat.2021.06.027>.
- C. Dai, T. Chu, X. Li, H. Jiang, T. Liu, Y. Zhou, L. Gao, C. Shen, J. Ge, A novel UV-curable extravascular stent to prevent restenosis of venous grafts, *Compos. B Eng.* 225 (2021), <https://doi.org/10.1016/j.compositesb.2021.109260>.
- C. Tianshu, G. Congrong, Z. Zhiwei, L. Fei, S. Ayu, Z. Yuanbiao, C. Jing, J. Ge, Rapamycin combined with α -cyanoacrylate contributes to inhibiting intimal hyperplasia in rat models, *Arq. Bras. Cardiol.* 112 (1) (2019) 3–10, <https://doi.org/10.5935/abc.20180247>.
- P. Zhao, Q. Yao, P.J. Zhang, E. The, Y. Zhai, L. Ao, M.J. Jarrett, C.A. Dinarello, D. A. Fullerton, X. Meng, Single-cell RNA-seq reveals a critical role of novel pro-inflammatory EndMT in mediating adverse remodeling in coronary artery-on-a-chip, *Sci. Adv.* 7 (34) (2021), <https://doi.org/10.1126/sciadv.abg1694>.
- Y. Ying, C.B. Sun, S.Q. Zhang, B.J. Chen, J.Z. Yu, F.Y. Liu, J. Wen, J. Hou, S.S. Han, J.Y. Yan, Z.S. Yang, L. Xiong, Induction of autophagy via the TLR4/NF- κ B signaling pathway by astragaloside IV contributes to the amelioration of inflammation in RAW264.7 cells, *Biomedicine & pharmacotherapy = Biomedecine & pharmacotherapie* 137 (2021), 111271, <https://doi.org/10.1016/j.biopha.2021.111271>.
- Z.S. Yang, J.Y. Yan, N.P. Han, W. Zhou, Y. Cheng, X.M. Zhang, N. Li, J.L. Yuan, Anti-inflammatory effect of Yu-Ping-Feng-San via TGF- β 1 signaling suppression in rat model of COPD, *Iranian journal of basic medical sciences* 19 (9) (2016) 993–1002.
- J.Z. Yu, Y. Ying, Y. Liu, C.B. Sun, C. Dai, S. Zhao, S.Z. Tian, J. Peng, N.P. Han, J. L. Yuan, J.Y. Yan, Z.S. Yang, Antifibrotic action of Yifei Sanjie formula enhanced autophagy via PI3K-AKT-mTOR signaling pathway in mouse model of pulmonary fibrosis, *Biomedicine & pharmacotherapy = Biomedecine & pharmacotherapie* 118 (2019), 109293, <https://doi.org/10.1016/j.biopha.2019.109293>.
- A. Isogai, T. Saito, H. Fukuzumi, TEMPO-oxidized cellulose nanofibers, *Nanoscale* 3 (1) (2011) 71–85, <https://doi.org/10.1039/c0nr00583e>.
- F.D. Li, S. Eagle, C. Brophy, K.M. Hocking, M. Osgood, P. Komalavilas, J. Cheung-Flynn, Pressure control during preparation of saphenous veins, *JAMA surgery* 149 (7) (2014) 655–662, <https://doi.org/10.1001/jamasurg.2013.5067>.

- [36] J. Zhao, J.J. Andreasen, J. Yang, B.S. Rasmussen, D. Liao, H. Gregersen, Manual pressure distension of the human saphenous vein changes its biomechanical properties-implication for coronary artery bypass grafting, *J. Biomech.* 40 (10) (2007) 2268–2276, <https://doi.org/10.1016/j.jbiomech.2006.10.014>.
- [37] S. Piera-Velazquez, S.A. Jimenez, Endothelial to mesenchymal transition: role in physiology and in the pathogenesis of human diseases, *Physiol. Rev.* 99 (2) (2019) 1281–1324, <https://doi.org/10.1152/physrev.00021.2018>.
- [38] Y. Li, K.O. Lui, B. Zhou, Reassessing endothelial-to-mesenchymal transition in cardiovascular diseases, *Nat. Rev. Cardiol.* 15 (8) (2018) 445–456, <https://doi.org/10.1038/s41569-018-0023-y>.
- [39] A.R. Palla, M. Ravichandran, Y.X. Wang, L. Alexandrova, A.V. Yang, P. Kraft, C. A. Holbrook, C.M. Schürch, A.T.V. Ho, H.M. Blau, Inhibition of prostaglandin-degrading enzyme 15-PGDH rejuvenates aged muscle mass and strength, *Science* (New York, N.Y.) 371 (6528) (2021), <https://doi.org/10.1126/science.abc8059>.
- [40] Y. Takagaki, S.M. Lee, Z. Dongqing, M. Kitada, K. Kanasaki, D. Koya, Endothelial autophagy deficiency induces IL6 - dependent endothelial mesenchymal transition and organ fibrosis, *Autophagy* 16 (10) (2020) 1905–1914, <https://doi.org/10.1080/15548627.2020.1713641>.
- [41] Q. Yang, D. Lei, S. Huang, Y. Yang, C. Jiang, H. Shi, W. Chen, Q. Zhao, Z. You, X. Ye, A novel biodegradable external stent regulates vein graft remodeling via the Hippo-YAP and mTOR signaling pathways, *Biomaterials* 258 (2020), 120254, <https://doi.org/10.1016/j.biomaterials.2020.120254>.
- [42] L. Ding, C. Hang, S. Cheng, L. Jia, L. Mou, L. Tang, C. Zhang, Y. Xie, W. Zheng, Y. Zhang, X. Jiang, A soft, conductive external stent inhibits intimal hyperplasia in vein grafts by electroporation and mechanical restriction, *ACS Nano* (2020), <https://doi.org/10.1021/acsnano.0c04827>.
- [43] W. Pachla, S. Przybysz, A. Jarzębska, M. Bieda, K. Sztwiertnia, M. Kulczyk, J. Skiba, Structural and mechanical aspects of hypoeutectic Zn-Mg binary alloys for biodegradable vascular stent applications, *Bioact. Mater.* 6 (1) (2021) 26–44, <https://doi.org/10.1016/j.bioactmat.2020.07.004>.
- [44] M. Tian, X. Wang, H. Sun, W. Feng, Y. Song, F. Lu, L. Wang, Y. Wang, B. Xu, H. Wang, S. Liu, Z. Liu, Y. Chen, Q. Miao, P. Su, Y. Yang, S. Guo, B. Lu, Z. Sun, K. Liu, C. Zhang, Y. Wu, H. Xu, W. Zhao, C. Han, X. Zhou, E. Wang, X. Huo, S. Hu, No-touch versus conventional vein harvesting techniques at 12 Months after coronary artery bypass grafting surgery: multicenter randomized, controlled trial, *Circulation* 144 (14) (2021) 1120–1129, <https://doi.org/10.1161/circulationaha.121.055525>.
- [45] A. Kulik, M.R. Le May, P. Voisine, J.C. Tardif, R. Delarochelliere, S. Naidoo, G. A. Wells, T.G. Mesana, M. Ruel, Aspirin plus clopidogrel versus aspirin alone after coronary artery bypass grafting: the clopidogrel after surgery for coronary artery disease (CASCADE) Trial, *Circulation* 122 (25) (2010) 2680–2687, <https://doi.org/10.1161/circulationaha.110.978007>.
- [46] I. Mylonaki, E. Allémann, F. Saucy, J.A. Haefliger, F. Delie, O. Jordan, Perivascular medical devices and drug delivery systems: making the right choices, *Biomaterials* 128 (2017) 56–68, <https://doi.org/10.1016/j.biomaterials.2017.02.028>.
- [47] B. Qiang, J. Toma, H. Fujii, A.B. Oshero, N. Nili, J.D. Sparkes, P. Fefer, M. Samuel, J. Butany, H. Leong-Poi, B.H. Strauss, Statin therapy prevents expansive remodeling in venous bypass grafts, *Atherosclerosis* 223 (1) (2012) 106–113, <https://doi.org/10.1016/j.atherosclerosis.2012.03.013>.
- [48] A. Forte, M. Grossi, K.M. Turczynska, K. Svedberg, B. Rinaldi, M. Donniacuo, A. Holm, B. Baldetorp, M. Vicchio, M. De Feo, P. Santè, U. Galderisi, L. Berrino, F. Rossi, P. Hellstrand, B.O. Nilsson, M. Cipollaro, Local inhibition of ornithine decarboxylase reduces vascular stenosis in a murine model of carotid injury, *Int. J. Cardiol.* 168 (4) (2013) 3370–3380, <https://doi.org/10.1016/j.ijcard.2013.04.153>.
- [49] S.C. Owen, H. Li, W.G. Sanders, A.K. Cheung, C.M. Terry, Correlation of tissue drug concentrations with in vivo magnetic resonance images of polymer drug depot around arteriovenous graft, *J. Contr. Release : official journal of the Controlled Release Society* 146 (1) (2010) 23–30, <https://doi.org/10.1016/j.jconrel.2010.05.005>.
- [50] R. Waksman, Update on bioabsorbable stents: from bench to clinical, *J. Intervent. Cardiol.* 19 (5) (2006) 414–421, <https://doi.org/10.1111/j.1540-8183.2006.00187.x>.
- [51] R. Curvello, V.S. Raghuvanshi, G. Garnier, Engineering nanocellulose hydrogels for biomedical applications, *Adv. Colloid Interface Sci.* 267 (2019) 47–61, <https://doi.org/10.1016/j.cis.2019.03.002>.
- [52] M. Ahearne, Introduction to cell-hydrogel mechanosensing, *Interface focus* 4 (2) (2014), 20130038, <https://doi.org/10.1098/rsfs.2013.0038>.
- [53] Y. Wu, X. Li, Y. Sun, X. Tan, C. Wang, Z. Wang, L. Ye, Multiscale design of stiffening and ROS scavenging hydrogels for the augmentation of mandibular bone regeneration, *Bioact. Mater.* 20 (2023) 111–125, <https://doi.org/10.1016/j.bioactmat.2022.05.021>.
- [54] C.Y. Zou, X.X. Lei, J.J. Hu, Y.L. Jiang, Q.J. Li, Y.T. Song, Q.Y. Zhang, J. Li-Ling, H. Q. Xie, Multi-crosslinking hydrogels with robust bio-adhesion and pro-coagulant activity for first-aid hemostasis and infected wound healing, *Bioact. Mater.* 16 (2022) 388–402, <https://doi.org/10.1016/j.bioactmat.2022.02.034>.
- [55] K. Prakobna, V. Kisonen, C. Xu, L.A. Berglund, Strong reinforcing effects from galactolucumannan hemicellulose on mechanical behavior of wet cellulose nanofiber gels, *J. Mater. Sci.* 50 (22) (2015) 7413–7423, <https://doi.org/10.1007/s10853-015-9299-z>.
- [56] J. Yang, F. Xu, C.R. Han, Metal ion mediated cellulose nanofibrils transient network in covalently cross-linked hydrogels: mechanistic insight into morphology and dynamics, *Biomacromolecules* 18 (3) (2017) 1019–1028, <https://doi.org/10.1021/acs.biomac.6b01915>.
- [57] J.S. Temenoff, A.G. Mikos, Review: tissue engineering for regeneration of articular cartilage, *Biomaterials* 21 (5) (2000) 431–440, [https://doi.org/10.1016/s0142-9612\(99\)00213-6](https://doi.org/10.1016/s0142-9612(99)00213-6).
- [58] D.W. Huttmacher, Scaffolds in tissue engineering bone and cartilage, *Biomaterials* 21 (24) (2000) 2529–2543, [https://doi.org/10.1016/s0142-9612\(00\)00121-6](https://doi.org/10.1016/s0142-9612(00)00121-6).
- [59] S.G. Priya, H. Jungvid, A. Kumar, Skin tissue engineering for tissue repair and regeneration, *Tissue engineering, Part B, Reviews* 14 (1) (2008) 105–118, <https://doi.org/10.1089/teb.2007.0318>.
- [60] Y. Lei, X. Wang, J. Liao, J. Shen, Y. Li, Z. Cai, N. Hu, X. Luo, W. Cui, W. Huang, Shear-responsive boundary-lubricated hydrogels attenuate osteoarthritis, *Bioact. Mater.* 16 (2022) 472–484, <https://doi.org/10.1016/j.bioactmat.2022.02.016>.
- [61] K. Liu, M. Wiendels, H. Yuan, C. Ruan, P.H.J. Kouwer, Cell-matrix reciprocity in 3D culture models with nonlinear elasticity, *Bioact. Mater.* 9 (2022) 316–331, <https://doi.org/10.1016/j.bioactmat.2021.08.002>.
- [62] M. Müller, E. Öztürk, Ø. Arlov, P. Gatenholm, M. Zenobi-Wong, Alginate sulfate-nanocellulose bioinks for cartilage bioprinting applications, *Ann. Biomed. Eng.* 45 (1) (2017) 210–223, <https://doi.org/10.1007/s10439-016-1704-5>.
- [63] S. Schwarz, H.M. Avila, N. Rotter, P. Gatenholm, 3D bioprinting of human chondrocyte-laden nanocellulose hydrogels for patient-specific auricular cartilage regeneration, *Tissue Eng.* 21 (2015), S373–S373.
- [64] K. Markstedt, A. Mantas, I. Tournier, H. Martínez Ávila, D. Hägg, P. Gatenholm, 3D bioprinting human chondrocytes with nanocellulose-alginate bioink for cartilage tissue engineering applications, *Biomacromolecules* 16 (5) (2015) 1489–1496, <https://doi.org/10.1021/acs.biomac.5b00188>.
- [65] G. Turnbull, J. Clarke, F. Picard, P. Riches, L. Jia, F. Han, B. Li, W. Shu, 3D bioactive composite scaffolds for bone tissue engineering, *Bioact. Mater.* 3 (3) (2018) 278–314, <https://doi.org/10.1016/j.bioactmat.2017.10.001>.
- [66] C. Wang, W. Huang, Y. Zhou, L. He, Z. He, Z. Chen, X. He, S. Tian, J. Liao, B. Lu, Y. Wei, M. Wang, 3D printing of bone tissue engineering scaffolds, *Bioact. Mater.* 5 (1) (2020) 82–91, <https://doi.org/10.1016/j.bioactmat.2020.01.004>.
- [67] K.H. Simons, A. de Jong, J.W. Jukema, M.R. de Vries, R. Arens, P.H.A. Quax, T cell co-stimulation and co-inhibition in cardiovascular diseases: a double-edged sword, *Nat. Rev. Cardiol.* 16 (6) (2019) 325–343, <https://doi.org/10.1038/s41569-019-0164-7>.
- [68] I. Xenogiannis, M. Zenati, D.L. Bhatt, S.V. Rao, J. Rodés-Cabau, S. Goldman, K. A. Shunk, K. Mavromatis, S. Banerjee, K. Alaswad, I. Nikolakopoulos, E. Vemmo, J. Arsanonyi, D. Alexopoulos, M.N. Burke, V.N. Bapat, E.S. Brilakis, Saphenous vein graft failure: from pathophysiology to prevention and treatment strategies, *Circulation* 144 (9) (2021) 728–745, <https://doi.org/10.1161/circulationaha.120.052163>.
- [69] J. Tejero, S. Shiva, M.T. Gladwin, Sources of vascular nitric oxide and reactive oxygen species and their regulation, *Physiol. Rev.* 99 (1) (2019) 311–379, <https://doi.org/10.1152/physrev.00036.2017>.
- [70] E.M. Ahmed, Hydrogel: preparation, characterization, and applications: a review, *J. Adv. Res.* 6 (2) (2015) 105–121, <https://doi.org/10.1016/j.jare.2013.07.006>.
- [71] Z. Li, Z. Chen, H. Chen, K. Chen, W. Tao, X.K. Ouyang, L. Mei, X. Zeng, Polyphenol-based hydrogels: pyramid evolution from crosslinked structures to biomedical applications and the reverse design, *Bioact. Mater.* 17 (2022) 49–70, <https://doi.org/10.1016/j.bioactmat.2022.01.038>.
- [72] M. Gonçalves da Costa Sousa, G. Conceição de Almeida, D.C. Martins Mota, R. Andrade da Costa, S.C. Dias, S.N. Limberger, F. Ko, L.T. Lin, E.F. Haney, H. Etayash, B. Baquir, M.J. Trimble, Y. Shen, Z. Su, M. Haapasalo, D. Pletzer, L. Chaves de Souza, G. Schuindt Teixeira, R.M. Silva, R.E.W. Hancock, O.L. Franco, T.M. Berto Rezende, Antibiofilm and immunomodulatory resorbable nanofibrous filling for dental pulp regenerative procedures, *Bioact. Mater.* 16 (2022) 173–186, <https://doi.org/10.1016/j.bioactmat.2022.01.027>.
- [73] R. Galante, T.J.A. Pinto, R. Colaço, A.P. Serro, Sterilization of hydrogels for biomedical applications: a review, *J. Biomed. Mater. Res., Part B* 106 (6) (2018) 2472–2492, <https://doi.org/10.1002/jbm.b.34048>.
- [74] R. Galante, D. Ghisleni, P. Paradiso, V.D. Alves, T.J.A. Pinto, R. Colaço, A.P. Serro, Sterilization of silicone-based hydrogels for biomedical application using ozone gas: comparison with conventional techniques, *Materials science & engineering, C, Materials for biological applications* 78 (2017) 389–397, <https://doi.org/10.1016/j.msec.2017.04.073>.
- [75] M.M. Pereira, N.R. Raposo, R. Brayner, E.M. Teixeira, V. Oliveira, C.C. Quintão, L. S. Camargo, L.H. Mattoso, H.M. Brandão, Cytotoxicity and expression of genes involved in the cellular stress response and apoptosis in mammalian fibroblast exposed to cotton cellulose nanofibers, *Nanotechnology* 24 (7) (2013), 075103, <https://doi.org/10.1088/0957-4484/24/7/075103>.
- [76] Y. Liu, Y. Sui, C. Liu, C. Liu, M. Wu, B. Li, Y. Li, A physically crosslinked polydopamine/nanocellulose hydrogel as potential versatile vehicles for drug delivery and wound healing, *Carbohydr. Polym.* 188 (2018) 27–36, <https://doi.org/10.1016/j.carbpol.2018.01.093>.
- [77] S. Napavichayanun, R. Yamdech, P. Aramwit, The safety and efficacy of bacterial nanocellulose wound dressing incorporating sericin and polyhexamethylene biguanide: in vitro, in vivo and clinical studies, *Arch. Dermatol. Res.* 308 (2) (2016) 123–132, <https://doi.org/10.1007/s00403-016-1621-3>.
- [78] I. Azoizis, J. Metcalfe, J. Reynolds, S. Keeton, S.S. Hakkii, J. Sheard, D. Wiedera, Three-dimensional cell culture of human mesenchymal stem cells in nanofibrillar cellulose hydrogels, *MRS Communications* 7 (3) (2017) 458–465, <https://doi.org/10.1557/mrc.2017.59>.
- [79] M. Bhattacharya, M.M. Malinen, P. Lauren, Y.R. Lou, S.W. Kuisma, L. Kanninen, M. Lille, A. Corlu, C. GuGuen-Guilouzo, O. Ikkala, A. Laukkanen, A. Urtti, M. Yliperttula, Nanofibrillar cellulose hydrogel promotes three-dimensional liver cell culture, *J. Contr. Release : official journal of the Controlled Release Society* 164 (3) (2012) 291–298, <https://doi.org/10.1016/j.jconrel.2012.06.039>.

- [80] Y.R. Lou, L. Kanninen, T. Kuisma, J. Niklander, L.A. Noon, D. Burks, A. Urtti, M. Yliperttula, The use of nanofibrillar cellulose hydrogel as a flexible three-dimensional model to culture human pluripotent stem cells, *Stem Cell. Dev.* 23 (4) (2014) 380–392, <https://doi.org/10.1089/scd.2013.0314>.
- [81] M.M. Malinen, L.K. Kanninen, A. Corlu, H.M. Isoniemi, Y.R. Lou, M.L. Yliperttula, A.O. Urtti, Differentiation of liver progenitor cell line to functional organotypic cultures in 3D nanofibrillar cellulose and hyaluronan-gelatin hydrogels, *Biomaterials* 35 (19) (2014) 5110–5121, <https://doi.org/10.1016/j.biomaterials.2014.03.020>.
- [82] L. Bao, J. Tang, F.F. Hong, X. Lu, L. Chen, Physicochemical properties and in vitro biocompatibility of three bacterial nanocellulose conduits for blood vessel applications, *Carbohydr. Polym.* 239 (2020), 116246, <https://doi.org/10.1016/j.carbpol.2020.116246>.
- [83] B. Thomas, M.C. Raj, A.K. B, R.M. H, J. Joy, A. Moores, G.L. Drisko, C. Sanchez, Nanocellulose, a versatile green platform: from biosources to materials and their applications, *Chem. Rev.* 118 (24) (2018) 11575–11625, <https://doi.org/10.1021/acs.chemrev.7b00627>.
- [84] J.A. Zepp, E.E. Morrissey, Cellular crosstalk in the development and regeneration of the respiratory system, *Nat. Rev. Mol. Cell Biol.* 20 (9) (2019) 551–566, <https://doi.org/10.1038/s41580-019-0141-3>.
- [85] D.E. Wagner, A.M. Klein, Lineage tracing meets single-cell omics: opportunities and challenges, *Nat. Rev. Genet.* 21 (7) (2020) 410–427, <https://doi.org/10.1038/s41576-020-0223-2>.
- [86] B.C. Cooley, J. Nevado, J. Mellad, D. Yang, C. St Hilaire, A. Negro, F. Fang, G. Chen, H. San, A.D. Walts, R.L. Schwartzbeck, B. Taylor, J.D. Lanzer, A. Wragg, A. Elagha, L.E. Beltran, C. Berry, R. Feil, R. Virmani, E. Ladich, J.C. Kovacic, M. Boehm, TGF- β signaling mediates endothelial-to-mesenchymal transition (EndMT) during vein graft remodeling, *Sci. Transl. Med.* 6 (227) (2014), <https://doi.org/10.1126/scitranslmed.3006927>, 227ra34.
- [87] T. Niida, K. Isoda, M. Kitagaki, N. Ishigami, T. Adachi, O. Matsubara, K. Takeda, T. Kishimoto, F. Ohsuzu, I κ BNS regulates interleukin-6 production and inhibits neointimal formation after vascular injury in mice, *Cardiovasc. Res.* 93 (2) (2012) 371–379, <https://doi.org/10.1093/cvr/cvr323>.
- [88] I. Zeller, M. Knoflach, A. Seubert, S.B. Kreutmayer, M.E. Stelzmüller, E. Wallnoefer, S. Blunder, S. Frotschnig, B. Messner, J. Willeit, P. Debbage, G. Wick, S. Kiechl, G. Laufer, D. Bernhard, Lead contributes to arterial intimal hyperplasia through nuclear factor erythroid 2-related factor-mediated endothelial interleukin 8 synthesis and subsequent invasion of smooth muscle cells, *Arterioscler. Thromb. Vasc. Biol.* 30 (9) (2010) 1733–1740, <https://doi.org/10.1161/atvbaha.110.211011>.
- [89] T. Saito, Y. Hasegawa, Y. Ishigaki, T. Yamada, J. Gao, J. Imai, K. Uno, K. Kaneko, T. Ogiwara, T. Shimosawa, T. Asano, T. Fujita, Y. Oka, H. Katagiri, Importance of endothelial NF- κ B signalling in vascular remodelling and aortic aneurysm formation, *Cardiovasc. Res.* 97 (1) (2013) 106–114, <https://doi.org/10.1093/cvr/cvs298>.
- [90] R.D. Rudic, D. Brinster, Y. Cheng, S. Fries, W.L. Song, S. Austin, T.M. Coffman, G. A. FitzGerald, COX-2-derived prostacyclin modulates vascular remodeling, *Circ. Res.* 96 (12) (2005) 1240–1247, <https://doi.org/10.1161/01.Res.0000170888.11669.28>.
- [91] S. Xue, X. Zhou, W. Sang, C. Wang, H. Lu, Y. Xu, Y. Zhong, L. Zhu, C. He, J. Ma, Cartilage-targeting peptide-modified dual-drug delivery nanoplatfrom with NIR laser response for osteoarthritis therapy, *Bioact. Mater.* 6 (8) (2021) 2372–2389, <https://doi.org/10.1016/j.bioactmat.2021.01.017>.
- [92] S. Ren, H. Zhang, Y. Mu, M. Sun, P. Liu, Pharmacological effects of Astragaloside IV: a literature review, *Journal of traditional Chinese medicine = Chung i tsa chih ying wen pan* 33 (3) (2013) 413–416, [https://doi.org/10.1016/s0254-6272\(13\)60189-2](https://doi.org/10.1016/s0254-6272(13)60189-2).
- [93] C. Xu, F. Tang, M. Lu, J. Yang, R. Han, M. Mei, J. Hu, M. Zhou, H. Wang, Astragaloside IV improves the isoproterenol-induced vascular dysfunction via attenuating eNOS uncoupling-mediated oxidative stress and inhibiting ROS-NF- κ B pathways, *Int. Immunopharm.* 33 (2016) 119–127, <https://doi.org/10.1016/j.intimp.2016.02.009>.
- [94] X. Chen, L.H. Peng, Y.H. Shan, N. Li, W. Wei, L. Yu, Q.M. Li, W.Q. Liang, J.Q. Gao, Astragaloside IV-loaded nanoparticle-enriched hydrogel induces wound healing and anti-scar activity through topical delivery, *Int. J. Pharm.* 447 (1–2) (2013) 171–181, <https://doi.org/10.1016/j.ijpharm.2013.02.054>.
- [95] M. Witting, K. Obst, W. Friess, S. Hedtrich, Recent advances in topical delivery of proteins and peptides mediated by soft matter nanocarriers, *Biotechnol. Adv.* 33 (6 Pt 3) (2015) 1355–1369, <https://doi.org/10.1016/j.biotechadv.2015.01.010>.